Characterization of phyllosilicates observed in the central Mawrth Vallis region, Mars, their potential formational processes, and implications for past climate

Nancy K. McKeown,[1] Janice L. Bishop,[2,3] Eldar Z. Noe Dobrea,[4] Bethany L. Ehlmann,[5] Mario Parente,[6] John F. Mustard,[5] Scott L. Murchie,[7] Gregg A. Swayze,[8] Jean-Pierre Bibring,[9] and Eli A. Silver[1]

Received 14 November 2008; revised 21 May 2009; accepted 22 July 2009; published 26 November 2009.

[1] Mawrth Vallis contains one of the largest exposures of phyllosilicates on Mars. Nontronite, montmorillonite, kaolinite, and hydrated silica have been identified throughout the region using data from the Compact Reconnaissance Imaging Spectrometer for Mars (CRISM). In addition, saponite has been identified in one observation within a crater. These individual minerals are identified and distinguished by features at 1.38–1.42, ~1.91, and 2.17–2.41 μm. There are two main phyllosilicate units in the Mawrth Vallis region. The lowermost unit is nontronite bearing, unconformably overlain by an Al-phyllosilicate unit containing montmorillonite plus hydrated silica, with a thin layer of kaolinite plus hydrated silica at the top of the unit. These two units are draped by a spectrally unremarkable capping unit. Smectites generally form in neutral to alkaline environments, while kaolinite and hydrated silica typically form in slightly acidic conditions; thus, the observed phyllosilicates may reflect a change in aqueous chemistry. Spectra retrieved near the boundary between the nontronite and Al-phyllosilicate units exhibit a strong positive slope from 1 to 2 μm, likely from a ferrous component within the rock. This ferrous component indicates either rapid deposition in an oxidizing environment or reducing conditions. Formation of each of the phyllosilicate minerals identified requires liquid water, thus indicating a regional wet period in the Noachian when these units formed. The two main phyllosilicate units may be extensive layers of altered volcanic ash. Other potential formational processes include sediment deposition into a marine or lacustrine basin or pedogenesis.

Citation: McKeown, N. K., J. L. Bishop, E. Z. Noe Dobrea, B. L. Ehlmann, M. Parente, J. F. Mustard, S. L. Murchie, G. A. Swayze, J.-P. Bibring, and E. A. Silver (2009), Characterization of phyllosilicates observed in the central Mawrth Vallis region, Mars, their potential formational processes, and implications for past climate, *J. Geophys. Res.*, *114*, E00D10, doi:10.1029/2008JE003301.

1. Introduction

[2] Mawrth Vallis is one of the oldest outflow channels on Mars and cuts through Noachian-aged terrain on the boundary between the southern highlands and northern lowlands, near 25°N, −20°E (Figure 1) [*Edgett and Parker*, 1997; *Scott and Tanaka*, 1986]. The Mawrth Vallis region contains one of the most extensive deposits of phyllosilicates on Mars, with detections across an area of approximately 1000 × 1000 km^2 (E. Z. Noe Dobrea et al., Mineralogy and stratigraphy of phyllosilicate-bearing and dark mantling units in the greater Mawrth Vallis/west Arabia Terra area: Constraints on geological origin, submitted to *Journal of Geophysical Research*, 2009). Phyllosilicate deposits have been identified only in early to middle Noachian–aged terrain, leading *Bibring et al.* [2006] to name this period the "phyllosian" era, characterized by nonacidic aqueous alteration. Multiple mechanisms could be responsible for this alteration including long-lasting, ambient temperature surface water, subsurface water mobilized by cratering, or hydrothermal processes [*Bibring et al.*, 2006]. As phyllosilicates only form by aqueous processes, their identification indicates the presence of liquid water in the geologic past.

[1]Department of Earth and Planetary Sciences, University of California, Santa Cruz, California, USA.
[2]SETI Institute Mountain View, California, USA.
[3]NASA Ames Research Center, Moffett Field, California, USA.
[4]Jet Propulsion Laboratory, California Institute of Technology, Pasadena, California, USA.
[5]Department of Geological Sciences, Brown University, Providence, Rhode Island, USA.
[6]Department of Electrical Engineering, Stanford University, Stanford, California, USA.
[7]Johns Hopkins University Applied Physics Laboratory, Laurel, Maryland, USA.
[8]U.S. Geological Survey, Denver, Colorado, USA.
[9]Institut d'Astrophysique Spatiale, Université Paris Sud, CNRS, Orsay, France.

0148-0227/09/2008JE003301

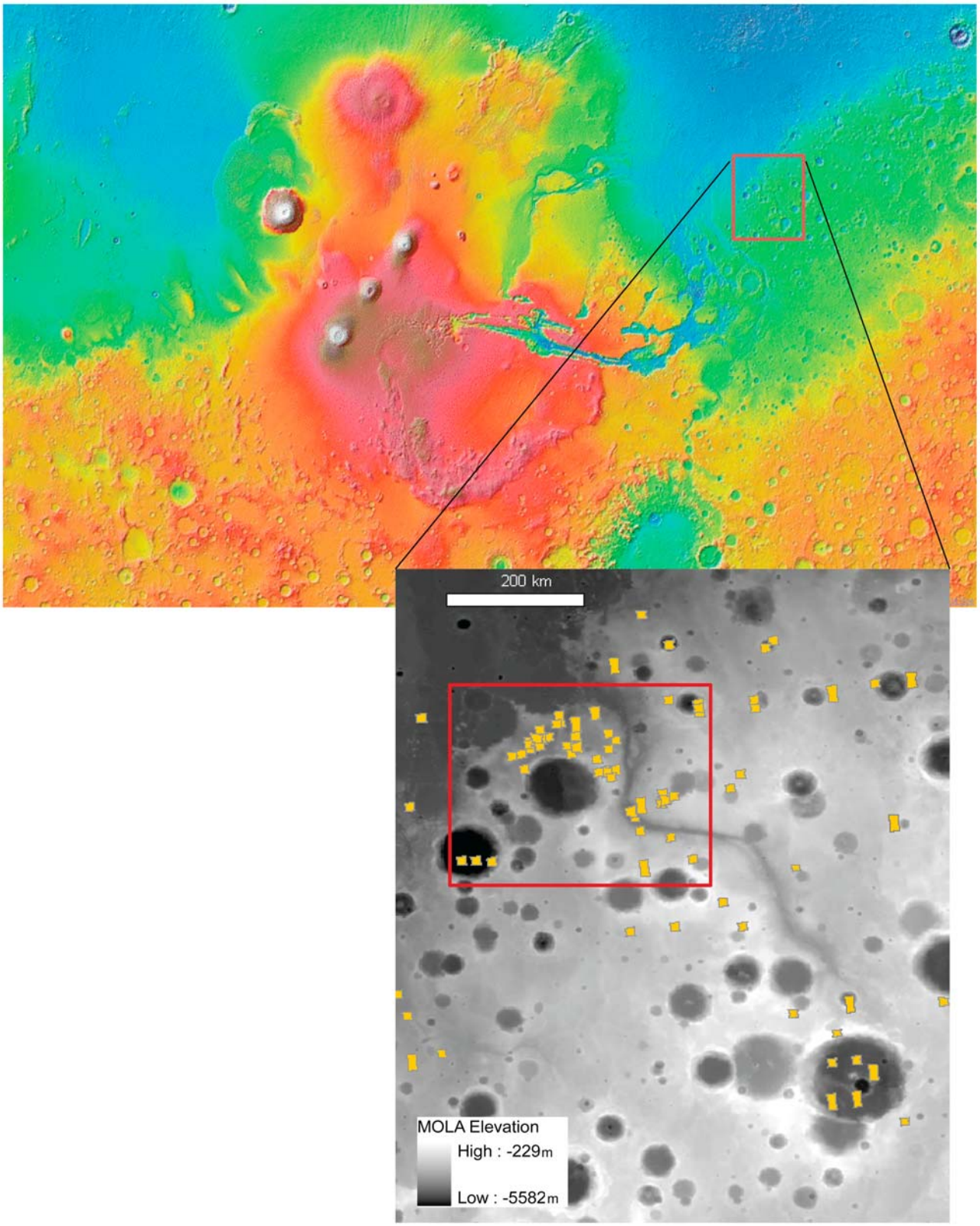

Figure 1. Location of Mawrth Vallis. The maps are MOLA elevation data, with white/red representing higher elevations and blue representing lower elevations. The red box in the inset indicates the central Mawrth Vallis area discussed in this paper and is ~350 km across. The gold symbols in the inset are CRISM image footprints.

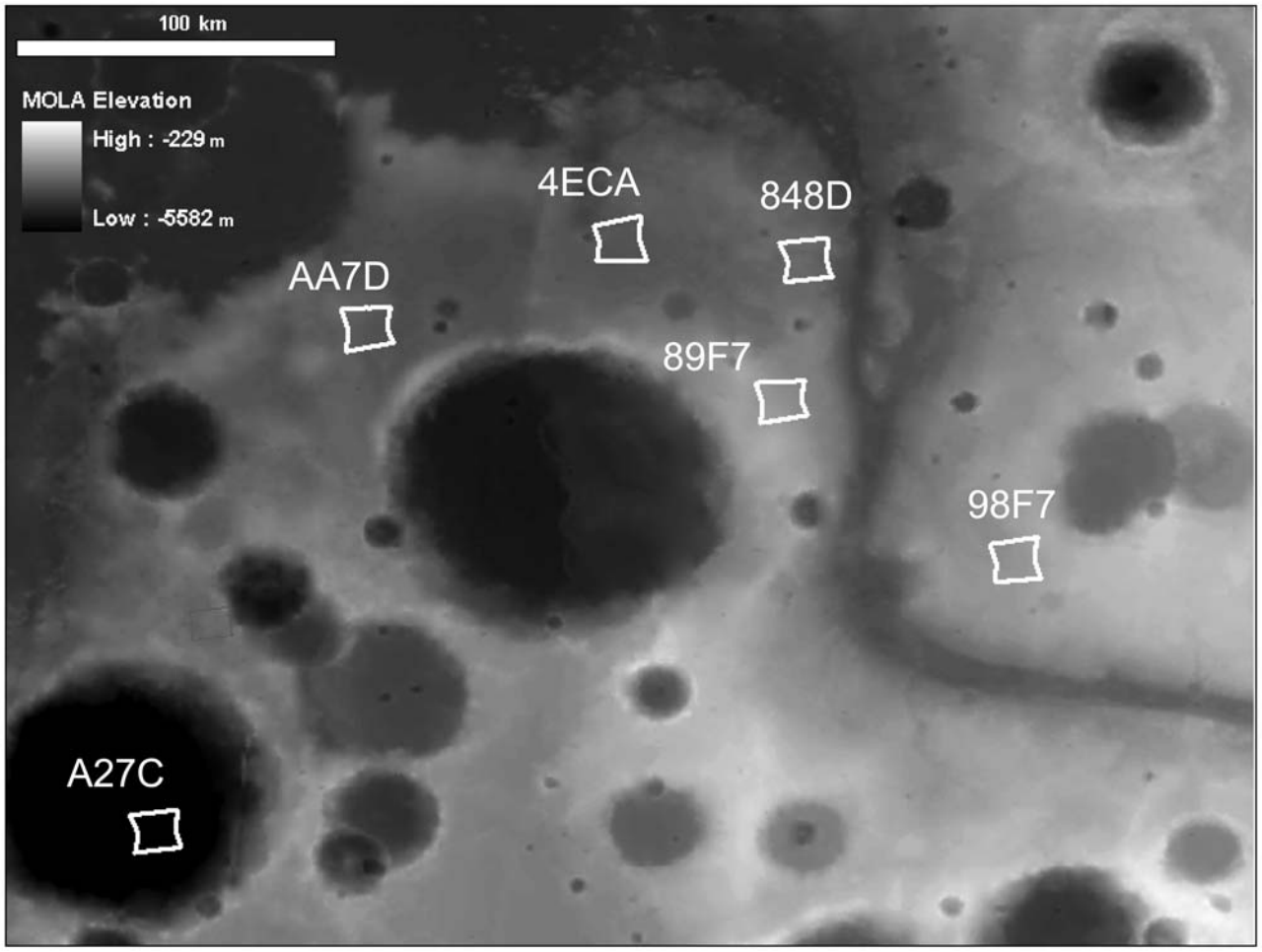

Figure 2. Location of the six images evaluated in this study displayed on MOLA elevation data, with higher elevations in white.

[3] In this paper, we examine six images from the Compact Reconnaissance Imaging Spectrometer for Mars (CRISM) which form a rough transect across the central Mawrth Vallis region (Figure 2) and characterize the mineralogy through analysis of spectral features in the visible to short-wave infrared (~0.4–4 μm). These features are attributed to electronic excitations of Fe, plus overtones and combinations of the H_2O vibrations and the metal-OH vibration. Images FRT000089F7 and FRT000098F7, located over potential Mars Science Laboratory (MSL) landing sites [*Golombek et al.*, 2008] and images FRT0000A27C, FRT0000AA7D, FRT00004ECA, and FRT0000848D illustrate the variation in mineralogies observed.

2. Background

2.1. Previous Detections by OMEGA and CRISM

[4] Observatoire pour la Mineralogie, L'Eau, les Glaces et l'Activité (OMEGA) on board Mars Express detected phyllosilicates in several locations, including Mawrth Vallis and Nili Fossae [*Bibring et al.*, 2005]. Nontronite and montmorillonite were identified as the primary clay minerals in the Mawrth Vallis region based on absorption features at 2.29 μm, and ~2.21 μm, respectively, and ~1.91 μm (Figure 3) [*Bibring et al.*, 2005; *Poulet et al.*, 2005]. The phyllosilicate deposits are found only in light-toned outcrops. No pyroxene has been identified in light-toned phyllosilicate outcrops and no phyllosilicates were identified in darker-toned regions with pyroxene [*Loizeau et al.*, 2007]. The different mineralogies identified with OMEGA correlate to layers of different colors in visible wavelengths as observed in High-Resolution Stereo Camera (HRSC, on board Mars Express) data [*Loizeau et al.*, 2009]. Correlation of OMEGA data with HRSC data also identified a consistent stratigraphy: Al-phyllosilicates overlying Fe/Mg-phyllosilicates [*Loizeau et al.*, 2009]. Detailed morphological analyses combining data from Mars Global Surveyor/Mars Orbiter Camera (MOC), OMEGA, HRSC, and Mars Odyssey/Thermal Emission Imaging System (THEMIS) have shown that the phyllosilicate outcrops are sedimentary in nature, layered at the meter scale, and the entire sequence is >150 m thick [*Loizeau et al.*, 2007; *Michalski and Noe Dobrea*, 2007]. Therefore, the phyllosilicates were probably a bulk component of the rocks prior to the erosion of the Mawrth Vallis channel [*Loizeau et al.*, 2007; *Poulet et al.*, 2005].

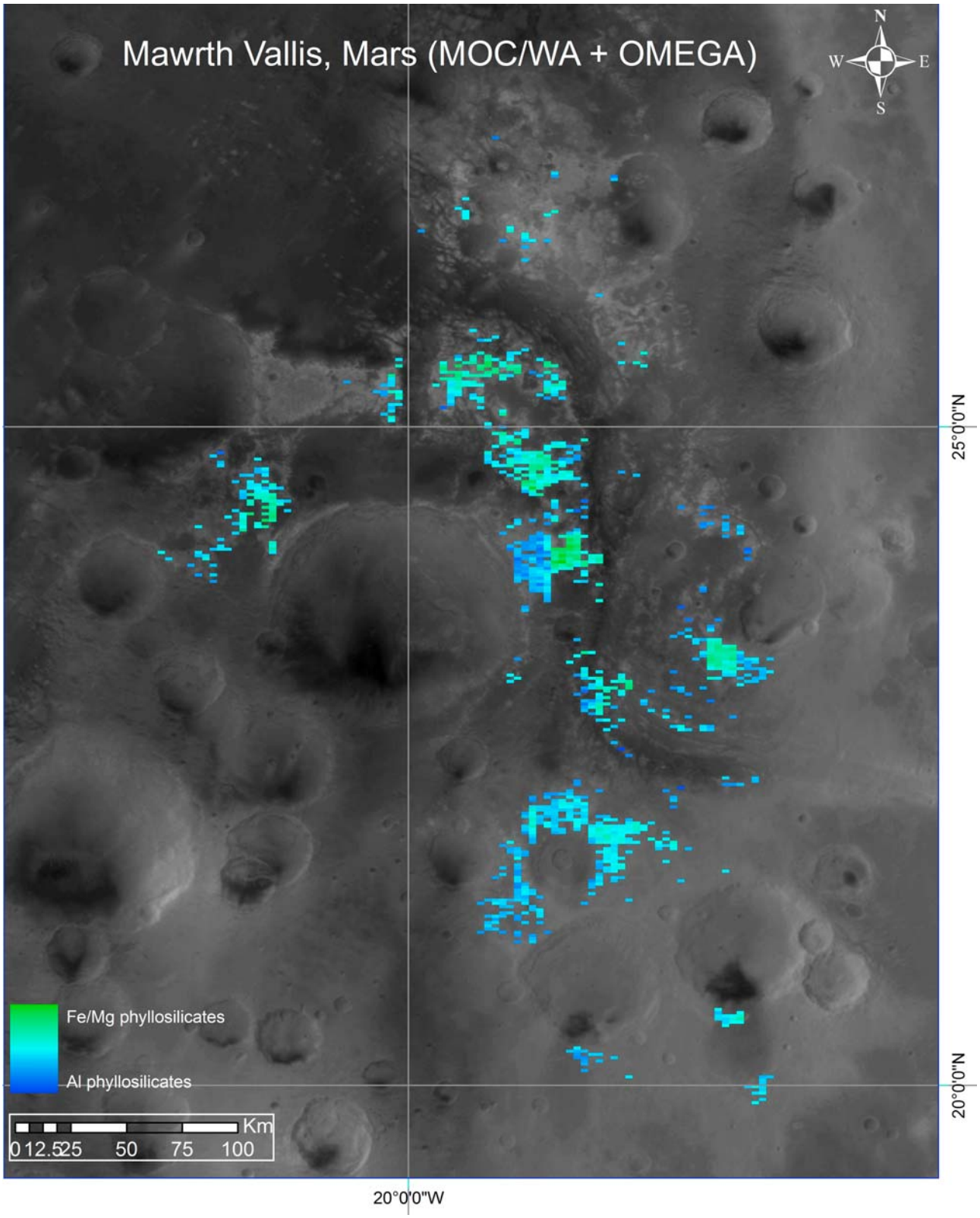

Figure 3. OMEGA data overlain on MOC wide angle. Fe/Mg-phyllosilicates are mapped in green, and Al-phyllosilicates and hydrated silica are mapped in blue. There is an excellent correlation between phyllosilicate detections and the light-toned material (E. Z. Noe Dobrea et al., submitted manuscript, 2009).

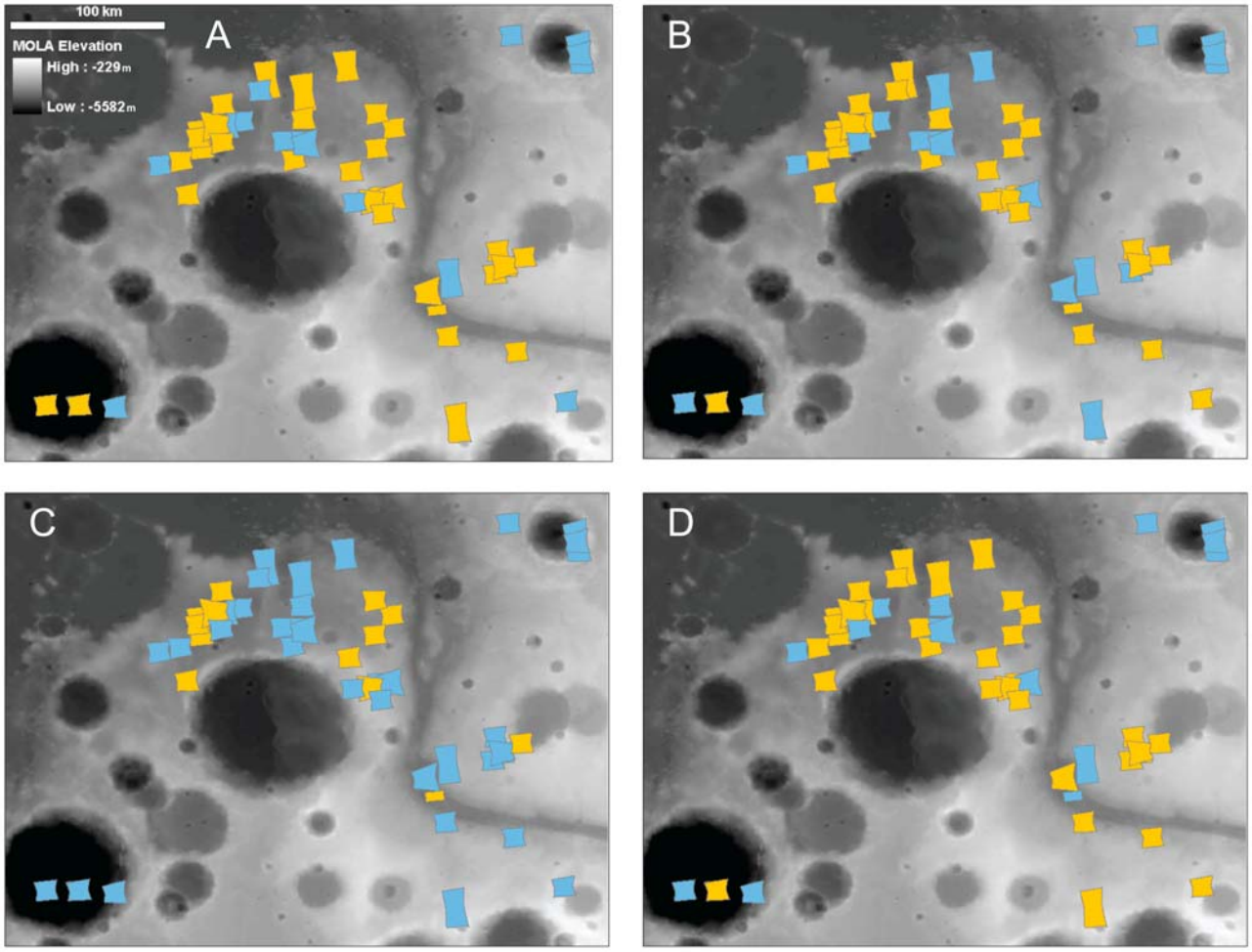

Figure 4. Maps of CRISM image footprints in the central Mawrth Vallis region. A yellow footprint indicates the presence of a given mineral in that image and blue indicates absence for (a) nontronite, (b) montmorillonite, (c) kaolinite, and (d) hydrated silica. Some footprints appear blue in all maps because there are no phyllosilicates present in that image. Image footprints are overlain on MOLA elevation data with white representing higher elevations. Scale bar is 100 km.

[5] CRISM data analysis have refined the OMEGA results, confirming the presence of nontronite and montmorillonite and further identifying a more Mg-rich nontronite, kaolinite, hydrated silica, and a ferrous component in many images (Figure 4) [*Bibring et al.*, 2005; *Bishop et al.*, 2007, 2008b; *Loizeau et al.*, 2007; *McKeown et al.*, 2007; *Noe Dobrea et al.*, 2007, 2008; *Poulet et al.*, 2005; *Wray et al.*, 2008]. CRISM data analyses also identified the same, consistent stratigraphy of Al-phyllosilicates overlying Fe/Mg-phyllosilicates, and further subdivided the Al-phyllosilicate unit into two layers: a kaolinite-bearing layer on top of a montmorillonite-bearing layer [*Bishop et al.*, 2008b; *Wray et al.*, 2008]. A ferrous phase has also been identified near the boundary between the two clay-bearing units [*Bishop et al.*, 2008b]. Combined CRISM and High Resolution Imaging Science Experiment, on board Mars Reconnaissance Orbiter (HiRISE) data analyses confirm that mineralogic differences correlate to color differences in the visible. Mars Orbiter Camera (MOC, on board Mars Global Surveyor) and HiRISE data have shown that the phyllosilicate units are layered at the meter scale [*Michalski and Noe Dobrea*, 2007; *Wray et al.*, 2008] and that the different mineralogies appear to have distinct textures: Fe/Mg-smectites have a polygonal fractured surface, montmorillonites have a smaller-scale polygonal fractured surface, hydrated silica and kaolinite both have smooth textures [*Bishop et al.*, 2008b].

[6] Several processes have been proposed for the formation of these units. Deposition of siliciclastics in an aqueous environment, alteration of volcanic ash, aeolian deposition of phyllosilicate-rich material, accumulation of altered ejecta, and alteration of primitive lava flows were suggested by *Loizeau et al.* [2007], favoring the first two hypotheses. *Michalski and Noe Dobrea* [2007] proposed a sedimentary or pyroclastic origin for these deposits and alteration either through diagenesis or transport from a clay source region. *Bishop et al.* [2008b] suggested that an ashfall deposit is the most likely precursor, and *Wray et al.* [2008] proposed a sedimentary or pyroclastic origin for the Al-phyllosilicate unit. In this study we examine the two most likely

Table 1. Depositional/Formational Alternatives for the Two Main Units Observed in the Mawrth Vallis Region With Implications for Water Source and Past Climate[a]

Unit	Formational/Depositional Process	Water Source	Climate
Nontronite	basaltic ashfall (bentonite)	groundwater/marine/lacustrine	active volcanism
	sedimentary deposition into a marine or lacustrine basin	marine/lacustrine basin	warm/wet, ongoing hydrolysis, possible seasonal dry periods
	pedogenesis of basaltic rocks	precipitation	warm/wet, ongoing hydrolysis, possible seasonal dry periods
Al-phyllosilicates	basaltic ashfall (bentonite)	groundwater/marine/lacustrine	active volcanism
	sedimentary deposition into a marine or lacustrine basin	marine/lacustrine basin	warm/wet, ongoing hydrolysis
	pedogenic leaching of nontronite	precipitation	warm/wet, ongoing hydrolysis

[a]Sources include *Righi and Meunier* [1995], *Keller* [1970], *Cole and Shaw* [1983], and *Ross and Shannon* [1926].

hypotheses in detail, ashfall and deposition in an aqueous environment, as well as pedogenesis.

2.2. Morphological Evidence for a Warm/Wet Mars

[7] Much evidence supports a warm, wet climate on early Mars [e.g., *Carr*, 1996]. Craters in the ancient highlands are flat floored and rimless, indicating substantial degradation has occurred. Craters in younger terrains and those superimposed on the degraded craters appear fresh, showing little sign of degradation, indicating that rates of erosion were higher on early Mars [*Craddock and Maxwell*, 1990]. Perhaps more critical are the myriad valley networks present in the ancient terrains [*Masursky*, 1973; *Pieri*, 1976]. It is likely that the valley networks were initiated by rainfall and surface runoff, then transitioned to groundwater sapping as the climate changed toward the end of the Noachian [*Craddock and Howard*, 2002; *Harrison and Grimm*, 2005]. Even during groundwater sapping, however, liquid water must have been stable at the surface for a period of time in order to form the channels [*Pieri*, 1980; *Squyres and Kasting*, 1994]. These factors suggest that Mars had a thicker atmosphere and warmer climate in the past [*Pollack*, 1979; *Pollack et al.*, 1987]. The detection of phyllosilicates is consistent with this theory because they form only in the extended presence of liquid water and therefore all the formational/depositional processes discussed here imply a wet climate (see Table 1 for a summary).

2.3. Remote Sensing of Clay Minerals

[8] *Chabrillat et al.* [2002] found that clay minerals could be successfully differentiated on Earth using an airborne hyperspectral sensor, such as AVIRIS or HyMap. They were able to accurately distinguish between montmorillonite, kaolinite, and mixed-layer illite/smectite clays. These minerals all have absorption features near 2.2 μm, but the absorptions have different shapes and there are additional absorption features at other wavelengths that were used to differentiate these three clay species [*Chabrillat et al.*, 2002; *Clark et al.*, 1990]. *Chabrillat et al.* [2002] found that having a high spectral resolution, particularly near 2.2 μm, is critical to identifying the smaller kaolinite doublet at 2.16 μm to distinguish it from montmorillonite and that a higher spatial resolution is critical for identification of purer and smaller outcrops. CRISM's spatial and spectral resolutions are both higher than OMEGA's thus facilitating identification of kaolinite outcrops that were not observed with OMEGA.

[9] However, there are some limitations. The visible/near-infrared–short wave infrared (VNIR-SWIR) wavelength region (0.4–3.0 μm) is excellent for identification of clay minerals because of the many absorption features due to OH and H_2O stretching and bending combinations and overtones [*Bishop et al.*, 1994; *Clark et al.*, 1990]; however, calculating the phyllosilicate abundance is more difficult. Minerals such as feldspars and quartz do not exhibit absorption features in the VNIR-SWIR, so they are not detectable by CRISM or OMEGA. Modeling by *Poulet et al.* [2008] based on VNIR-SWIR OMEGA data suggests that a "flat" component such as plagioclase feldspar (15–35%) is required in order to match the spectra observed by OMEGA and that 20–65% nontronite may be present. Analysis of Thermal Emission Spectrometer (TES) and Thermal Emission Imaging System (THEMIS) data over this region also indicates that feldspar and a silicate component such as opal is present [*Michalski and Fergason*, 2009]. A positive detection of phyllosilicate using spectroscopic data acquired at thermal wavelengths has been challenging, although recent work suggests the presence of altered silicate phases which may include phyllosilicates [*Michalski and Fergason*, 2009; *Ruff and Hamilton*, 2009]. Recent work by *Ruff and Hamilton* [2009] indicates that dioctahedral smectites such as montmorillonite may be apparent in TES spectra but at abundances near the TES detection limit of 10–20% in a $\sim 3 \times 6$ km^2 pixel. In light of these limitations, our paper focuses on the identification and geologic relationships among alteration phases, rather than their abundance.

3. Data and Methods

[10] Full-resolution targeted MRO-CRISM images (FRT's) consist of 544 channels covering the spectral range from 0.36 to 3.92 μm at a spectral sampling of 6.5 nm, in $\sim$10–12 km wide swaths at $\sim$18 m/pixel. The spectral data were collected by two detectors: a VNIR detector covering 0.36–1.05 μm and a SWIR detector covering 1.00–3.92 μm (Figure 5) [*Murchie et al.*, 2007]. CRISM data were converted to reflectance by subtracting the instrument background, dividing by processed measurements of the internal calibration standard, and dividing by solar irradiance

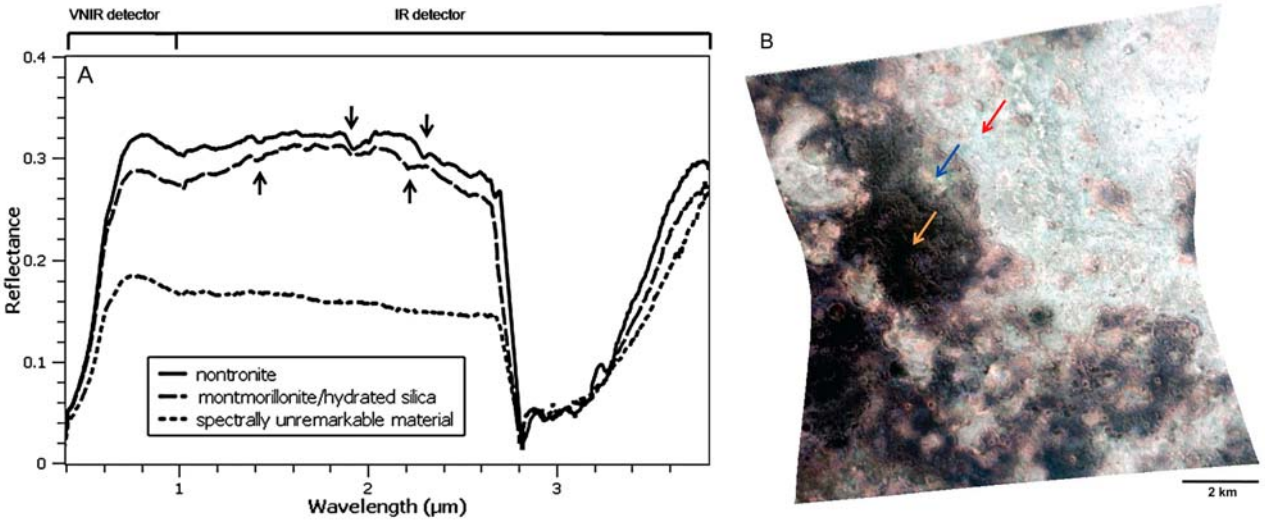

Figure 5. (a) Complete CRISM spectra from image FRT000098F7, taken from locations indicated by arrows on Figure 5b. Spectra are nonratioed 3 × 3 pixel averages. The VNIR detector measures from 0.39 to 1.01 μm, and the SWIR detector measures from 1.0 to 4.0 μm. Differences in detected reflectance and overlap at ~1 μm cause the slight offset observed. Arrows indicate key phyllosilicate vibration features (from left to right): ~1.4 μm combination H_2O stretch and bend and OH stretch overtone, ~1.9 μm H_2O combination bend overtone, ~2.21 μm Al-OH or Si-OH combination stretch and bend overtone, and ~2.3 μm Fe-OH or Mg-OH stretch and bend overtone. (b) False color IR image FRT000098F7 (R, 2.53 μm; G, 1.51 μm; B, 1.01 μm). Arrows indicate location of spectra in Figures 5a and 11. Red arrow, nontronite; blue arrow, montmorillonite/hydrated silica; orange arrow, spectrally unremarkable capping unit.

[*Murchie et al.*, 2007, 2009]. Variations in illumination geometry were corrected by dividing I/F by the cosine of the incidence angle (derived from MOLA gridded topography at 128 pixels/degree). Atmospheric molecular opacity effects were minimized by dividing by a scaled atmospheric transmission spectrum derived from observations over Olympus Mons [*Mustard et al.*, 2008]. Images were then processed using a cleaning algorithm to remove noise and large spikes within the data due to instrument effects [*Parente*, 2008]. Band math calculations were performed to create a set of parameter maps that highlight specific spectral features [*Pelkey et al.*, 2007], used to identify regions of interest for further detailed analyses. Similar products are available online at http://crism-map.jhuapl.edu/. Finally, data from the two detectors were spliced to enable examination of complete CRISM spectra (M. Parente et al., Decomposition of mineral absorption bands using nonlinear least squares curve fitting: Applications to Martian meteorite and CRISM data, submitted to *Remote Sensing of Environment*, 2009).

[11] Spectra were retrieved in several ways: (1) a spectrum was taken directly from the data, usually of a 3 × 3 pixel or 5 × 5 pixel average to reduce noise; (2) a 3 × 3 pixel or 5 × 5 pixel spectrum was taken of the region of interest and of a spectrally unremarkable region within the same column; these were then ratioed, with the spectrum of interest in the numerator, to reduce systematic instrument noise (Figure 6); or (3) an average spectrum was retrieved from a region of interest (ROI) of the mineralogy, containing at least 60 points, and a second spectrum was calculated from a spectrally unremarkable ROI. These were then ratioed. This method was used when there were few spectrally unremarkable regions in an image or when the mineralogy of interest was a long, narrow exposure, as in a crater wall. Taking an average spectrum of a large ROI greatly reduces any column-specific noise so ratios can be calculated using spectra from different parts of the image.

4. Spectral Results and Discussion

[12] In Mawrth Vallis, large (>1.3 × 10^5 m^2) exposures of phyllosilicates are common. One of the largest continuous exposures is found at MSL landing site 2 (Figure 7). In this mosaic, there is a large patch of nontronite in the eastern part (orange/red). This grades gradually upward and outward through ferrous-bearing layers (green), to the montmorillonite-bearing unit (cyan/blue). The slopes in landing site 2 are all <5°, except for the walls in a small crater that are 5–10° [*Beyer and the HiRISE Team*, 2008]. These low slopes are common throughout the central Mawrth Vallis region, though some outcrops do have steeper slopes. In FRT000089F7, FRT000098F7, and FRT0000AA7D (Figures 8a–8c), we observed a nontronite exposure with smaller outcrops of overlying Al-phyllosilicates on the edges. The unit beneath the nontronite is not exposed. In FRT00004ECA and FRT0000848D (Figures 8d and 8e), the nontronite exposures are smaller and the Al-phyllosilicate exposures are larger, likely because the Al-phyllosilicate unit has not been as extensively eroded as in the sites shown in first three images. In FRT0000A27C (Figure 8f), only very small exposures (a few 10s of m across) of phyllosilicates have been exhumed.

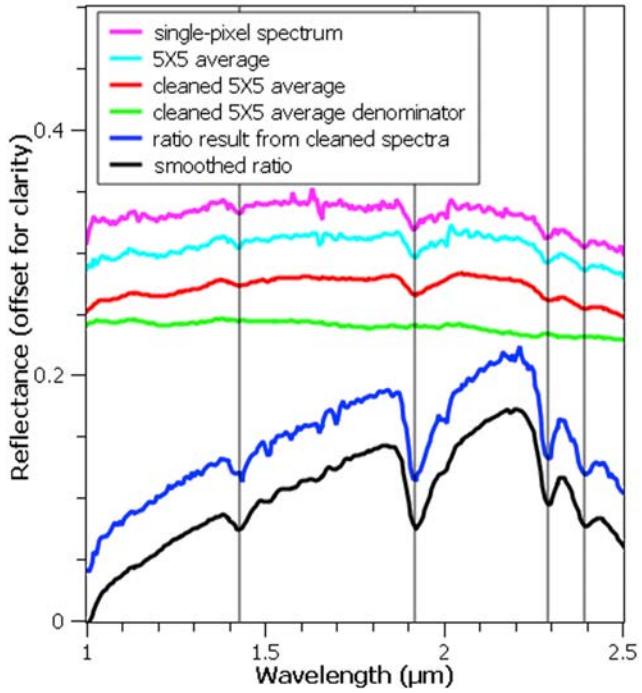

Figure 6. Plot illustrating the methods used to retrieve spectra from each image using a nontronite spectrum from FRT000098F7. The pink spectrum is from a single pixel. The absorptions at 1.42 μm, 1.91 μm, 2.29 μm, and 2.39 μm (marked by vertical lines) are observed, and much noise is present. The light blue spectrum is a 5 × 5 average centered on the same pixel; the noise is reduced and the absorption features are clearer than in the single-pixel spectrum. The red spectrum is the same 5 × 5 average after denoising and despiking algorithms have been applied [*Parente*, 2008], removing much of the noise. The green spectrum is a cleaned 5 × 5 average of spectrally unremarkable material used in the denominator of the ratio. The dark blue spectrum is the ratio result using the cleaned 5 × 5 average spectra, and the absorptions are much clearer, sharper, and deeper than in the nonratioed spectra. The black spectrum is the ratio result after five-point smoothing, which provides a nice clear spectrum with little noise.

4.1. VNIR Detector Spectral Results

[13] False color CRISM VNIR detector images (Figure 9c) as well as HRSC and HiRISE data of Mawrth Vallis [*Loizeau et al.*, 2007; *Wray et al.*, 2008] show substantial color variation, indicating textural changes or compositional diversity. Absorption features in the visible/near infrared (VNIR; 0.4–1.0 μm) region are due to Fe^{2+}-Fe^{3+} and Fe-O charge transfers and crystal field transitions [*Burns*, 1993; *Hunt*, 1977]. Nontronite is a dominantly Fe-bearing smectite, whereas montmorillonite is a dominantly Al-bearing smectite which may sometimes have minor Fe substitution of Al in the octahedral sites. These phyllosilicates have distinctly different spectral shapes in the 0.4–1.0 μm range (Figure 10). Nontronite often exhibits a shoulder at ~0.45 μm, an absorption at ~0.64 μm, and a broad absorption at ~0.94 μm [*Sherman and Vergo*, 1988]. Montmorillonite has none of these features, but does occasionally present a weak shoulder at ~0.50 μm, likely due to Fe substituting for Al as mentioned above. However, iron oxides exhibit band minima for wavelengths <1.0 μm at similar positions as nontronite (Figure 10) and commonly co-occur with phyllosilicates in terrestrial samples, also as products of alteration processes (e.g., in the Clay Mineral Society NG-1 nontronite source clay [*Lear et al.*, 1988] and the KGa kaolinite source clays [*Moll*, 2001]). Goethite, hematite, and lepidocrocite have minima near 0.53 μm. Hematite, goethite, and many other iron oxides and iron sulfates exhibit minima in the 0.85–0.95 μm range [*Morris et al.*, 2000]. The spectral signatures of these Fe oxides, either intimately mixed with the clays or coating the clays, can dominate the spectral features at <1.0 μm [*Parente et al.*, 2008]. Thus broad, iron-related absorption features and sharp vibrational absorption features are often treated separately in VNIR spectral analysis [*Clark et al.*, 2003].

[14] We mapped absorption band depths and spectral slope shortward of 1.0 μm using CRISM VNIR data from Mawrth Vallis to assess whether mineralogic changes in iron-bearing phases follow the major unit boundaries delineated by clay mineralogy (e.g., for FRT000098F7 in Figure 9). Three data parameters, band depth at 0.53 μm (BD530), shoulder height at 0.60 μm (SH600) and band depth at 0.86 μm (BD860), show systematic spatial variation, uncorrelated with albedo (Figure 9d). In nonratioed spectra, absorptions at <1.0 μm are subdued to absent, probably due to the dominating influence of Martian dust on spectral properties (Figure 11), although subtle shifts in the position of the reflectance maximum are observed.

[15] Examination of ratioed spectra averaged from ROIs of spectrally different regions in Figures 9c and 9d shows that iron-related absorptions apparently occur and vary independently of hydrated silicate-related spectral features. The spectra in Figures 9e and 9f were ratioed to the dark cap unit (green and cyan) to highlight spectral differences. The cap unit itself is not entirely homogeneous, varying from black to light green in the VNIR color composite (Figure 9c) and from light green-blue to yellow in the VNIR parameter composite (Figure 9d). Ratio spectra of the cap unit show that brightening is accompanied by the appearance of a band near 0.53 μm (green versus cyan versus maroon spectra in Figure 9f). Within the clay-bearing units, some areas which are strong in D2300 display diagnostic bands of nontronite at 1.9, 2.3, and 2.4 but lack absorptions at <1.0 μm (blue spectrum in Figures 9e and 9f). However, other spectra with less apparent nontronite bands (weaker 1.9 μm band and no 2.4 μm band) have a broad concavity, centered near 0.86 in continuum-removed spectra and a reflectance maximum at 0.76 μm. These features are diagnostic of red hematite [*Morris et al.*, 2000]. This hematite-bearing unit maps as magenta (elevated BD530 and BD860) in Figure 9d, salmon-colored in the false color IR map (Figure 9a), and appears beneath the cap unit, ringing erosional windows and overlying the nontronite unit. Areas with strong BD2200 appear yellow-green in the parameter map and also exhibit a broad absorption feature near 0.9 μm. No diagnostic mineral identification can be made from this combination of features.

[16] We attribute most of the variation in VNIR detector data to ferric oxides. Like *Wray et al.* [2008], who observed Fe oxide variation associated with Al phyllosilicates, we

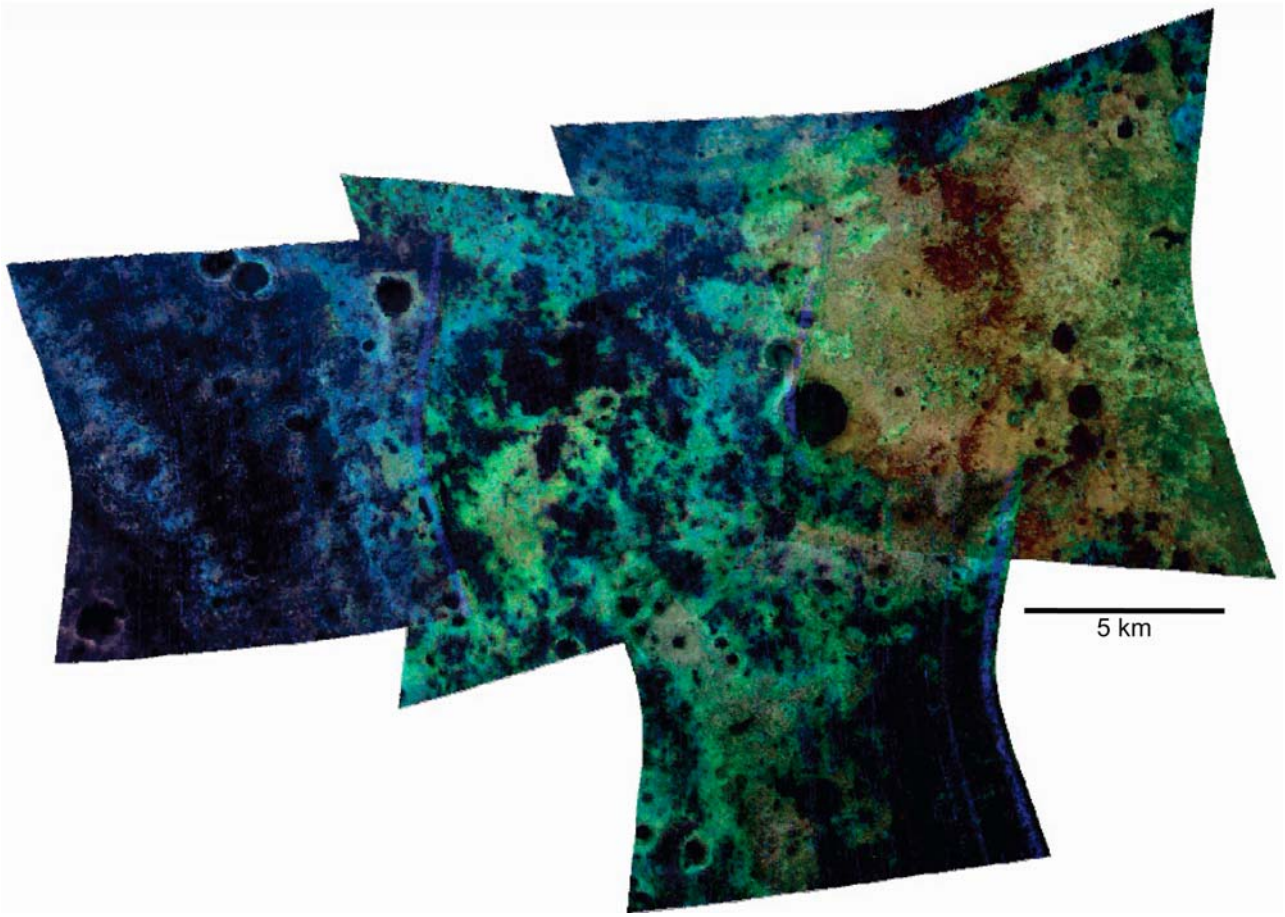

Figure 7. Mosaic of landing site 2 at Mawrth Vallis containing extensive contiguous phyllosilicate deposits. Parameter maps (R, D2300; G, OLINDEX; B, BD2210) are overlain on CRISM false color IR images (R, 2.53 μm; G, 1.51 μm; B, 1.01 μm) to better illustrate the texture of the units. Nontronite-bearing regions are orange, nontronite plus a ferrous component appears yellow, montmorillonite/hydrated silica plus a ferrous component appears green, montmorillonite/hydrated silica appears cyan, and kaolinite appears dark blue.

find variation in spectral properties at <1.0 um in both nontronite and Al phyllosilicate units. Spectral properties are not consistent with ferrous mafic minerals like olivine and pyroxenes. Hematite is clearly present in a unit or units underlying the cap unit but overlying the nontronite. That the spatial variation spectral properties at <1.0 μm does not follow the clay unit boundaries suggests that either the alteration process which produced the clays generated stratigraphic variation in Fe oxide composition or that the Fe oxides were produced by alteration separate from the principle clay unit formation.

4.2. IR Detector Spectral Results

[17] Spectral features from 1.0 to 2.5 μm are primarily due to overtones of vibrational processes within the structure of a mineral [*Hunt*, 1977]. Absorptions near 1.4 μm are combinations of the H_2O stretching (ν_1 or ν_3) and bending modes (ν_2) and of the structural hydroxyl (OH) stretch overtone ($2\nu_{OH}$) [*Bishop et al.*, 1994], and those near 1.9 μm are combinations of the H_2O stretching plus bending overtones ($\nu_1 + \nu_2$ or $\nu_3 + \nu_2$). In this study, we will refer to the absorptions due to H_2O vibrations as "hydration absorptions" because they indicate the presence of H_2O in the

Figure 8. (left) False color infrared composites (R, 2.53 μm; G, 1.51 μm; B, 1.01 μm) and (right) parameter maps (R, D2300; G, OLINDEX; B, BD2210 all stretched to exclude data <0) of the six images discussed in this paper, each ~10 km across (scale bar in lower corner is the same for all images). (a) FRT000089F7, (b) FRT000098F7, (c) FRT0000AA7D, (d) FRT00004ECA, (e) FRT0000848D, and (f) FRT0000A27C. In the false color composites, nontronite generally appears gray, montmorillonite plus hydrated silica appears light blue, kaolinite plus hydrated silica appears dark blue, and the capping unit is dark brown/black. Saponite in image FRT0000A27C (Figure 8f) appears lime green. In the parameter maps, nontronite appears orange, nontronite plus a ferrous component appears yellow, montmorillonite/hydrated silica plus a ferrous component appears green, montmorillonite/hydrated silica appears cyan, kaolinite appears dark blue, and saponite in FRT0000A27C (Figure 8f) appears fluorescent green. Residual blue striping in some parameter maps is due to instrument artifacts.

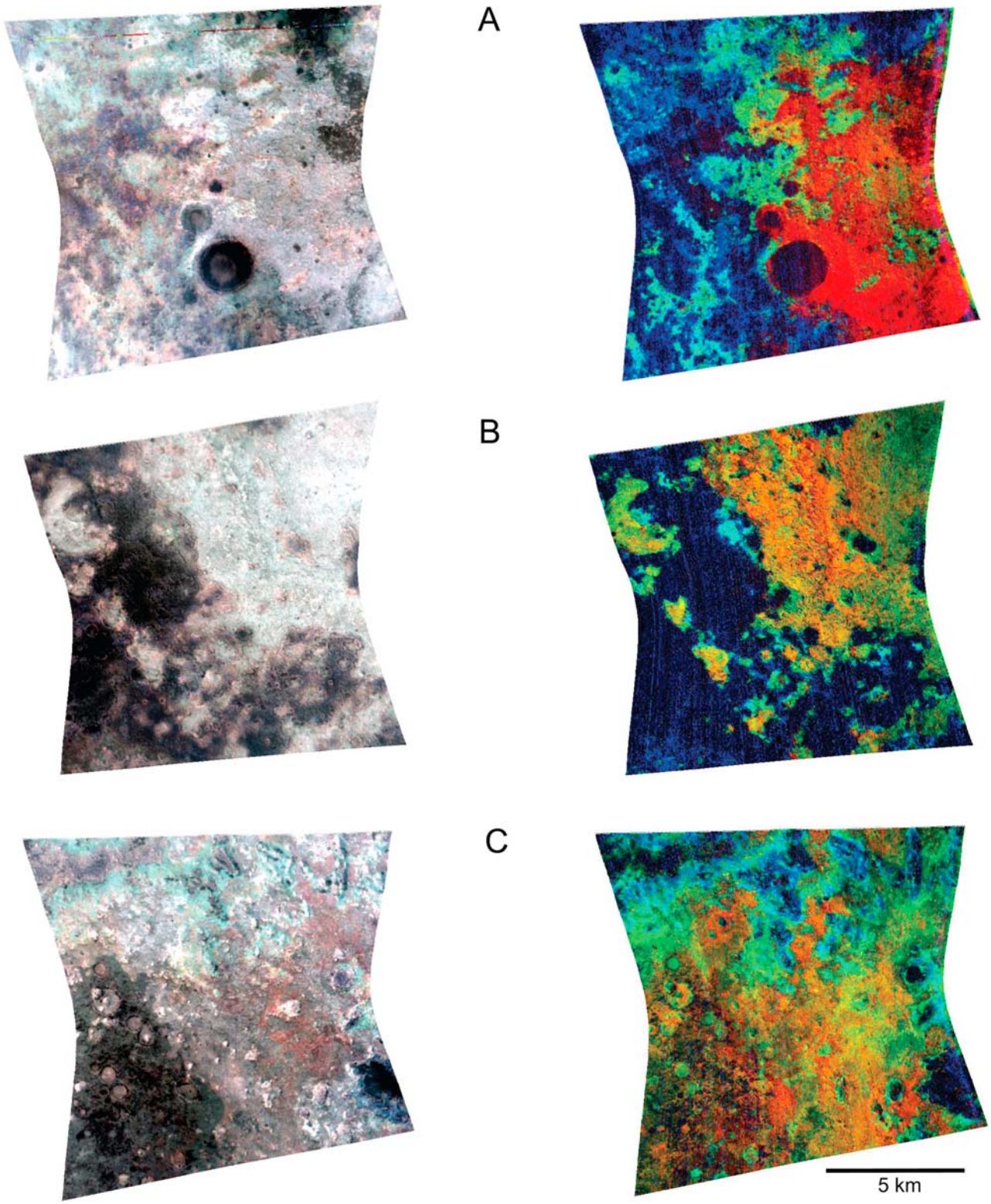

Figure 8

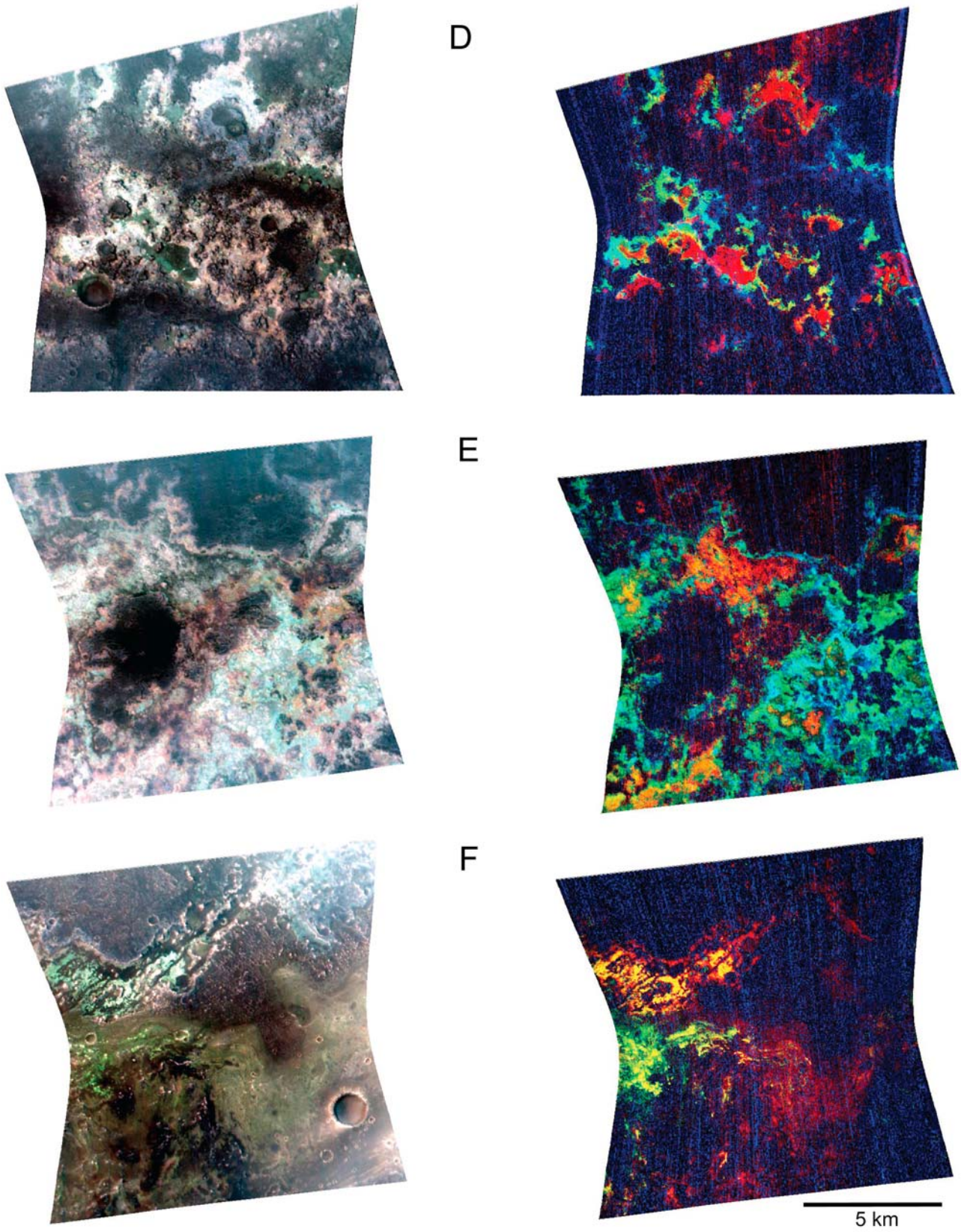

Figure 8. (continued)

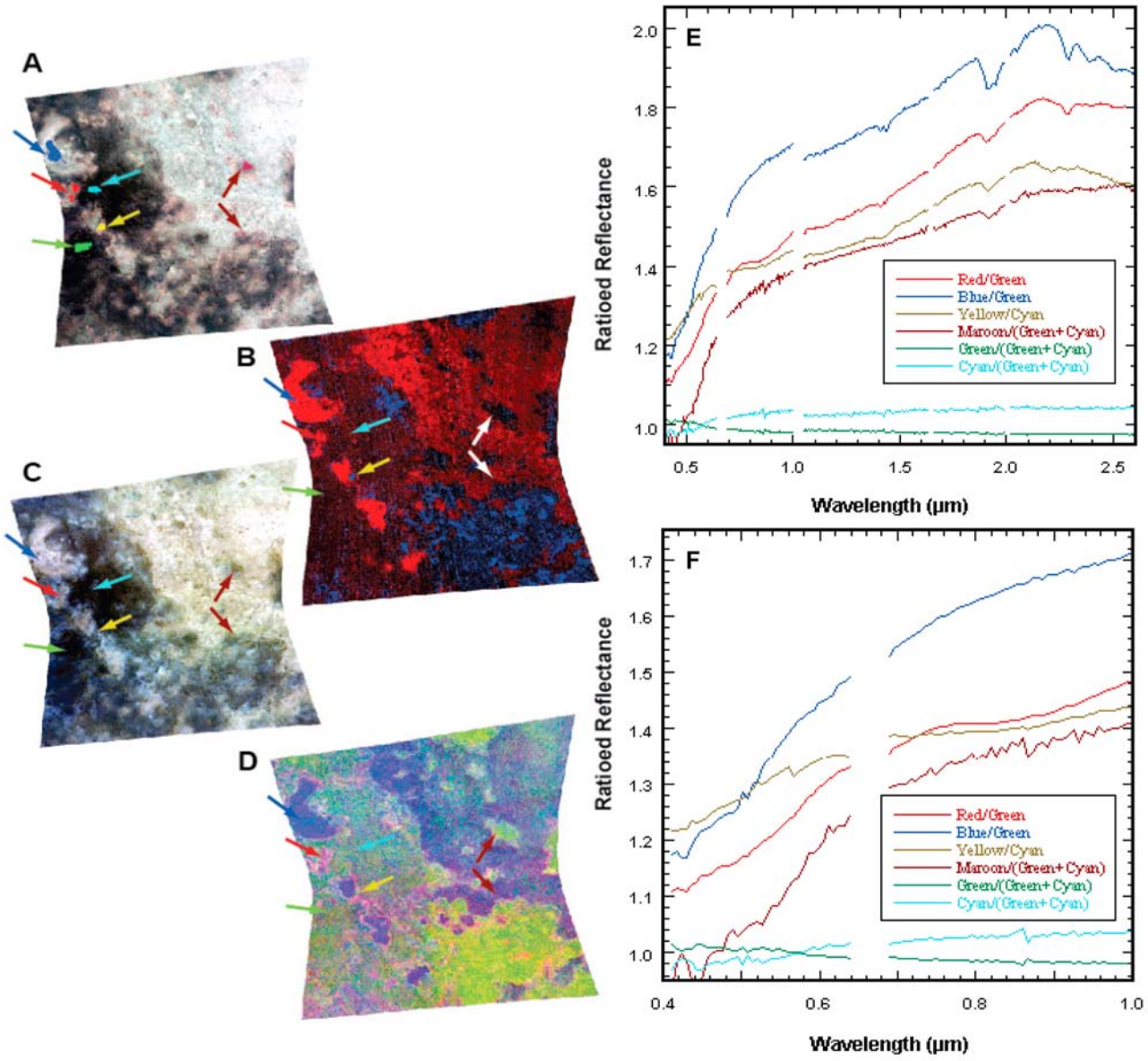

Figure 9. CRISM false color composites, parameter maps, and spectra from FRT00098F7. Arrows on the CRISM images indicate the locations of the regions of interest (ROIs) for spectra on the right. (a) False color composite from the SWIR detector (R, 2.38; G, 1.80; B, 1.15 μm) showing pixels defining the ROIs averaged to produce the spectra. (b) SWIR parameter map (R, D2300 (0.005–0.04 stretch); G, none; B, BD2200 (0.005–0.015 stretch)) showing the principal locations of the 2.3 and 2.2 μm absorptions due to nontronite and Al/Si hydrated silicates. (c) VNIR detector false color composite (R, 0.84; G, 0.68; B, 0.53 μm). (d) VNIR parameter map (R, BD860 (−0.019–0.0 stretch); G, SH600 (1.154–1.19 stretch); B, BD530 (0.083–0.181 stretch)) showing systematic variation in VNIR detector parameters. (e) Ratioed CRISM spectra of the ROIs from 0.4 to 2.6 μm. (f) Ratioed CRISM spectra of the ROIs from 0.4 to 1.0 μm showing variation in spectral slope and subtle, broad absorptions centered near 0.53 and 0.86 μm.

mineral either in the interlayer region or adsorbed on the surface. Absorptions in the 2.2 to 2.3 μm region are due to combinations of the stretching and bending vibrations of OH in the octahedral layer ($\nu_{OH} + \delta_{OH}$) [*Bishop et al.*, 1994; *Clark et al.*, 1990; *Hunt*, 1977]. Absorptions near 2.2 μm are due to Al-OH or Si-OH stretching and bending combinations, those near 2.28–2.29 μm are due to Fe-OH, and those near 2.30–2.31 μm are due to Mg-OH (e.g., Figure 5a). Table 2 lists specific mineral absorption features and band assignments: beidellite spectrum from *Gates* [2005]; kaolin family spectra from G. Swayze [*Clark et al.*, 2007]; saponite from USGS spectral library [*Clark et al.*, 1993]; montmorillonite, nontronite, and ferrous phyllosilicates from *Bishop et al.* [2008a]. Differences in band depth and band shape allow identification of different minerals with absorptions at the same wavelength. For

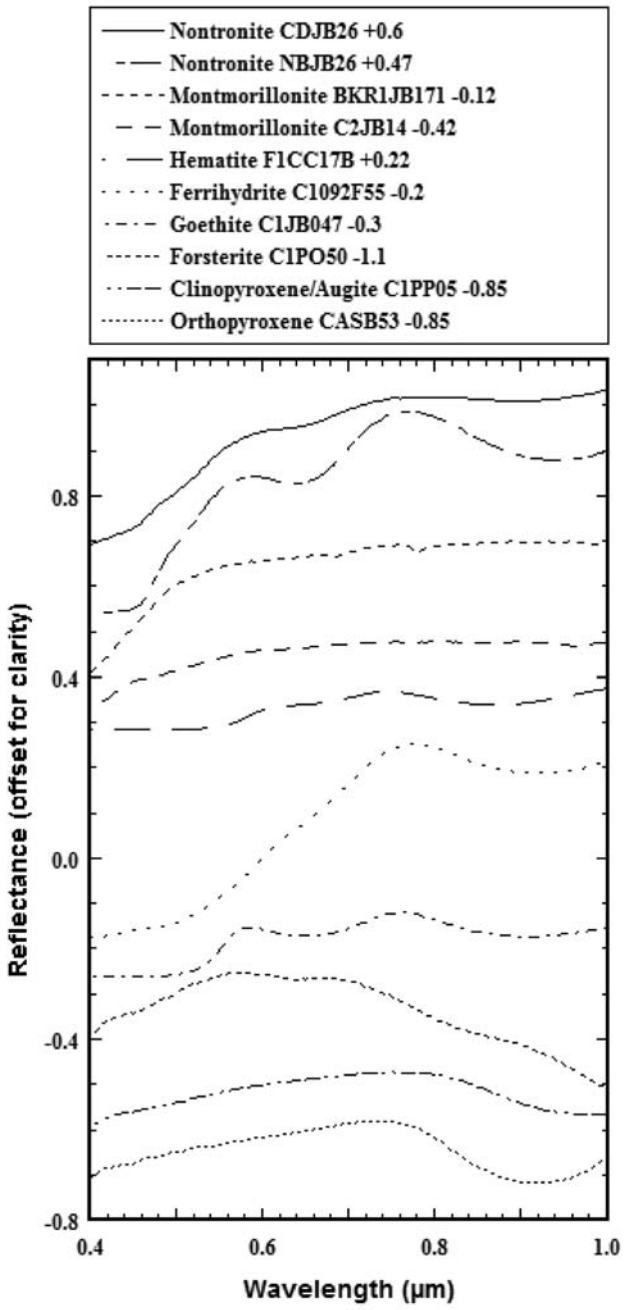

Figure 10. VNIR spectra of minerals from the CRISM spectral library [*Murchie et al.*, 2007]. Fe-related absorptions are sometimes apparent over the 0.4 to 1.0 μm wavelength range, measured by the CRISM VNIR detector.

example, montmorillonite, kaolinite, and hydrated silica (e.g., opal) all have absorptions centered near 2.21 μm. However, montmorillonite exhibits a sharp, deep absorption, kaolinite exhibits a doublet, and hydrated silica exhibits a broad shallow absorption which allows us to distinguish between them (Figure 12).

4.2.1. Nontronite

[18] Nontronite is the most common phyllosilicate identified in the Mawrth Vallis region and spectra retrieved from several images exhibit similar features (Figure 13a). Nontronite has hydration absorptions at 1.42 μm and 1.91 μm, an Fe-OH absorption at 2.29 μm, and other absorptions at 2.41 μm and 2.51 [e.g., *Bishop et al.*, 2008a]. In the Mawrth Vallis region, the Fe-OH stretch plus bend combination overtone is present at 2.28 μm or 2.29 μm, but most commonly at 2.29 μm. The shift in position of this band to 2.29 μm and sometimes 2.30 μm indicates some magnesium is present in the octahedral sites, substituting for iron. However, the position of the 1.42 μm band does not shift to shorter wavelengths, indicating the mineral is still nontronite rather than saponite or hectorite, other smectites with an Mg-OH absorption feature at ~2.30–2.31 μm. Additionally, some nontronite spectra retrieved near the boundary with the Al-phyllosilicate layer have a strong positive slope from 1 to 2 μm. This slope is attributed to a ferrous component as discussed in section 4.2.6.

4.2.2. Montmorillonite

[19] Montmorillonite has hydration absorptions at 1.41 μm and 1.92 μm and a sharp Al-OH absorption at 2.21 μm. The montmorillonite spectra observed at Mawrth Vallis in this study exhibit broader bands at ~2.2 μm than laboratory spectra indicating that it may be mixed with another mineral, such as opal or another form of hydrated silica with a broad feature at the same wavelength. *McKeown et al.* [2008] showed this effect with spectra of lab mixtures of montmorillonite, hydrated volcanic glass (obsidian), and hydrated silica from altered volcanic ash. Mixtures of hydrated ash or glass with at least 50% montmorillonite

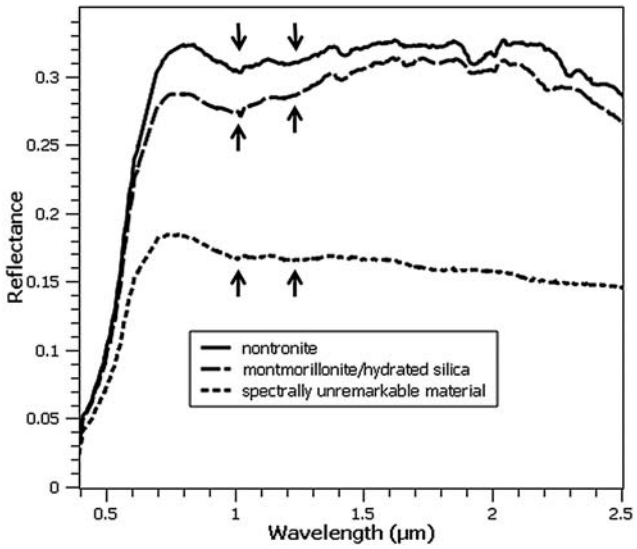

Figure 11. Spliced, nonratioed VNIR/SWIR spectra from FRT000098F7, taken from locations indicated by arrows on Figure 5b. Arrows indicate two broad features common to both the phyllosilicate spectra and the spectrally unremarkable capping unit. Additionally, the spectral shapes <1.0 μm show only subtle differences. There are differences in albedo (the capping unit is much darker than the clay spectra), and the nontronite spectrum has a maximum reflectance at a longer wavelength (0.83 μm) than the montmorillonite/hydrated silica or capping unit spectra (0.76 μm).

Table 2. Key SWIR Absorptions of Phyllosilicates Discussed in This Study and Their Vibrational Source[a]

Mineral	H_2O	OH	H_2O	Si-OH	Al-OH	Fe-OH	Mg-OH
Saponite	1.41	1.39	1.91				2.31
Nontronite	1.41	1.42	1.91			2.29, 2.41	
Beidellite	1.41	1.40	1.91		2.19		
Montmorillonite	1.41	1.41	1.91		2.21		
Hydrated silica	1.41	1.39	1.93 (weak)	2.21 (broad)			
Kaolinite		1.41			2.16 + 2.21 doublet		
Halloysite	1.41	1.39 (doublet with 1.41)	1.91		2.17 + 2.21 doublet		

[a]Short wave infrared (SWIR) absorptions measured in μm. H_2O band at 1.41 μm is weaker than the OH band at 1.39–1.42 μm and thus the H_2O band is frequently weak or absent in CRISM spectra.

showed features characteristic of montmorillonite at 2.2 μm while mixtures containing at least 80% hydrated ash or glass (less than 20% montmorillonite) were characterized by a broader feature here. Therefore, a mixture of hydrated silica and montmorillonite may be responsible for the broadened montmorillonite feature observed in the CRISM data (Figure 13b). Spectra of both montmorillonite and hydrated silica retrieved near the boundary with the underlying nontronite layer sometimes exhibit a strong positive slope from 1 to 2 μm attributed to a ferrous component.

4.2.3. Hydrated Silica

[20] Hydrated silica has weak 1.39 and 1.93 μm absorptions and a broad 2.21 μm Si-OH absorption [*Anderson and Wickersheim*, 1964; *Bishop et al.*, 2004; *Milliken et al.*, 2008]. The 2.21 μm feature typically extends out to 2.3 μm, unlike the montmorillonite which does not extend beyond 2.28 μm (Figure 13b). In Mawrth Vallis we observe in many locations a broadened feature near 2.21 μm that extends to 2.3 μm. Frequently, these are characterized by an OH overtone band at 1.39 μm rather than 1.41 μm as observed for montmorillonite. Also, the band strength at 1.93 μm relative to 2.21 μm is weaker for the units dominated by hydrated silica (Figure 13b).

4.2.4. Kaolinite

[21] Minerals of the kaolin family have similar, but not identical features. Kaolinite has an absorption at 1.4 μm absorption and an asymmetric doublet at 2.16 and 2.21 μm due to Al-OH overtones [e.g., *Bishop et al.*, 2008a; *Petit et al.*, 1999]. Dickite has an asymmetric doublet at 1.38 and 1.41 μm and a doublet at 2.18 and 2.21 μm. Halloysite has a doublet at 1.39 and 1.41 μm and a doublet at 2.17 and 2.21 μm where the 2.17 μm feature is a shoulder on the deeper 2.21 μm absorption. Halloysite also has a strong 1.91 μm absorption, unlike the other kaolin minerals. Nacrite has an asymmetric 1.38 and 1.41 μm absorption and a doublet at 2.18 and 2.20 μm with near-equal band depths.

[22] In the CRISM data, a doublet similar to kaolinite is present at 2.16 μm and 2.21 μm, but is broader than laboratory spectra, particularly toward longer wavelengths. A weak 1.41 μm band is present as well as a sharp 1.9 μm band, normally absent in kaolinite (Figure 13c). The band centers are consistent with the presence of kaolinite, and the altered features may be caused by a mixture of kaolinite with hydrated silica or halloysite which contains structural H_2O.

[23] Spectra of lab mixtures of kaolinite with hydrated silica showed a decrease in the kaolinite 2.2 μm band depth when less than 50% kaolinite is present [*McKeown et al.*, 2008]. Mixtures with montmorillonite showed a broadening of the 2.2 μm feature in kaolinite, also when less than 50% kaolinite is present [*Amador et al.*, 2009]. In both cases, the 2.16 μm doublet feature is still evident as an absorption or shoulder down to 25% kaolinite, with no shifting. Also, the 1.9 μm feature normally absent in kaolinite is prominent in mixture spectra even with only 15% montmorillonite or hydrated silica [*Amador et al.*, 2009; *McKeown et al.*, 2008]. Therefore, it seems likely that the CRISM spectra are mixtures of kaolinite with another hydrated Si- or Al-bearing phase.

4.2.5. Saponite

[24] Saponite has hydration absorptions at 1.39 μm and 1.91 μm and an Mg-OH absorption at 2.31 μm (Figure 13d). These features are distinct from the nontronite absorptions at nearby wavelengths. A spectrum with features characteristic of saponite is observed in data from image FRT0000A27C, within a ~80 km diameter crater. Because it is located on the floor of a crater, further investigation is needed to determine whether it was deposited at the same time as the layered phyllosilicate units nearer to the Mawrth Vallis

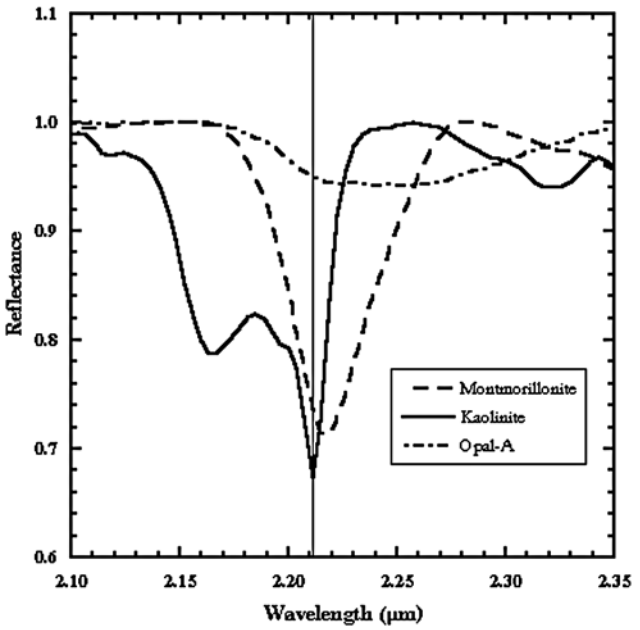

Figure 12. Continuum-removed laboratory spectra of montmorillonite, kaolinite, and hydrated silica (opal-A) showing clear differences in the 2.21 μm absorptions. Opal-A spectrum from *Bishop et al.* [2005].

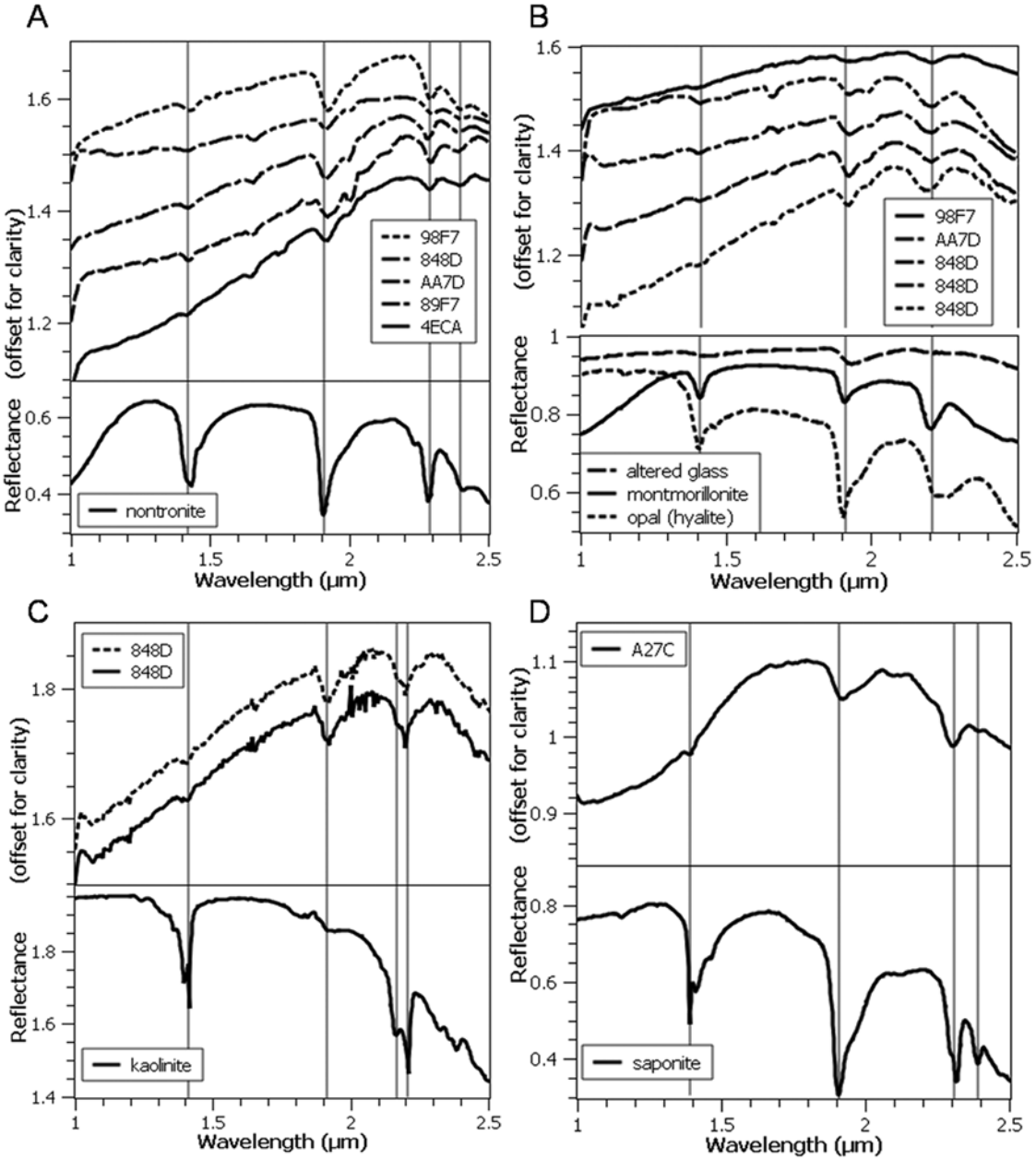

Figure 13. Spectral ratios of the mineralogies observed in Mawrth Vallis. The top half of each plot contains spectra retrieved from the CRISM images noted in the legend and the bottom half contains a laboratory spectrum of the identified mineral. (a) Nontronite has been observed in all images containing phyllosilicates; examples are shown here. Vertical lines mark absorption features at 1.42, 1.91, 2.29, and 2.40 μm. (b) Examples of montmorillonite and hydrated silica spectra. Vertical lines at 1.41, 1.91, and 2.21 μm. (c) Examples of kaolinite spectra. Vertical lines at 1.41, 1.91, 2.17, and 2.21 μm. (d) Example saponite spectrum. Vertical lines at 1.39, 1.91, 2.31, and 2.39 μm. All spectra are ratios and smoothed using a moving window average to reduce noise. Kaolinite spectra are not smoothed since smoothing removes the weak absorption feature at 2.16 μm.

channel or afterward as a result of the impact or another process. Spectra of this saponite-bearing unit also exhibit a slope from 1 to 2 μm consistent with a ferrous phase and a band at 2.5 μm characteristic of some smectites but also zeolites and carbonates. Continued analyses are needed in order to identify the other phases in this saponite-bearing unit.

4.2.6. Ferrous Component

[25] Some spectra observed in Mawrth Vallis have a strong positive slope from ~1–2 μm that is characteristic of ferrous (Fe^{2+}) bearing minerals. This slope is 2–5 times greater than in other Mawrth Vallis spectra (Figure 14). In ferrous minerals, this slope results from multiple, overlapping broad absorptions due to electronic excitations of

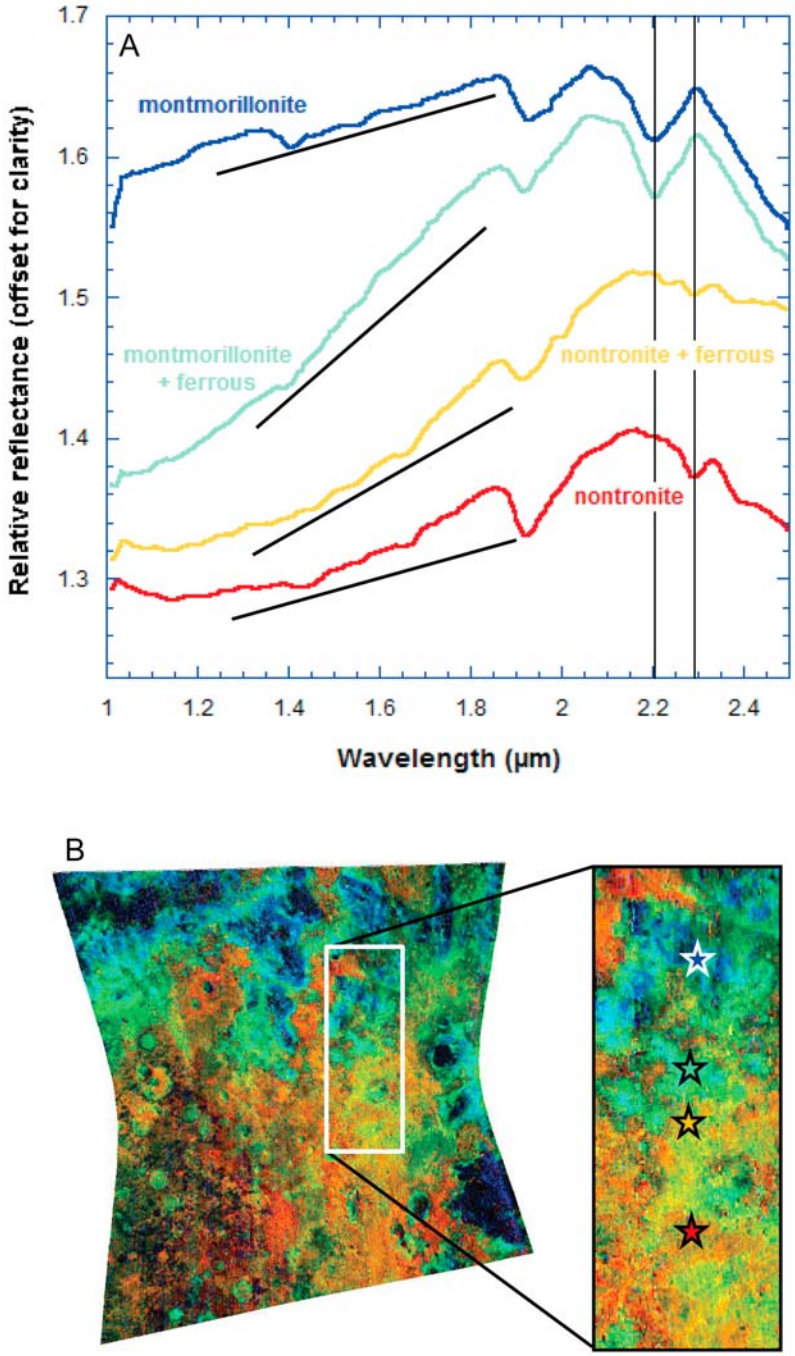

Figure 14. Spectra from FRT0000AA7D demonstrating the change in slope from 1 to 2 μm when a ferrous component is present. (a) From bottom to top: Red, nontronite; yellow-orange, nontronite + ferrous component; blue-green, montmorillonite + ferrous component; blue, montmorillonite. All spectra are 3 $\times$ 3 averages and were ratioed to the same denominator. The black lines indicate the approximate slope, which is 2–5 times steeper when a ferrous component is present than in nonferrous-bearing spectra. Colors match the locations shown in Figure 14b. (b) Parameter map of FRT0000AA7D (colors as in Figure 8). Stars in the inset indicate locations of spectra shown in Figure 14a from bottom to top: Red, nontronite; orange, nontronite + ferrous component; blue-green, montmorillonite + ferrous; blue, montmorillonite.

Fe^{2+}. These occur near 0.95–1.3 μm and are observed for minerals such as olivine, pyroxene, oxides, carbonates, and sulphates [*Burns*, 1993]. The strong 1–2 μm slope attributed to a ferrous component is typically observed at the boundary of the nontronite and montmorillonite-bearing units (Figure 15). Possible components that could cause this slope include olivine, ferrous chlorites, and ferrous micas. The spectrum of Fe^{2+}-bearing olivine has a strong positive slope from ~1–2 μm due to a strong absorption centered between 1.04 μm and 1.08 μm and a weaker

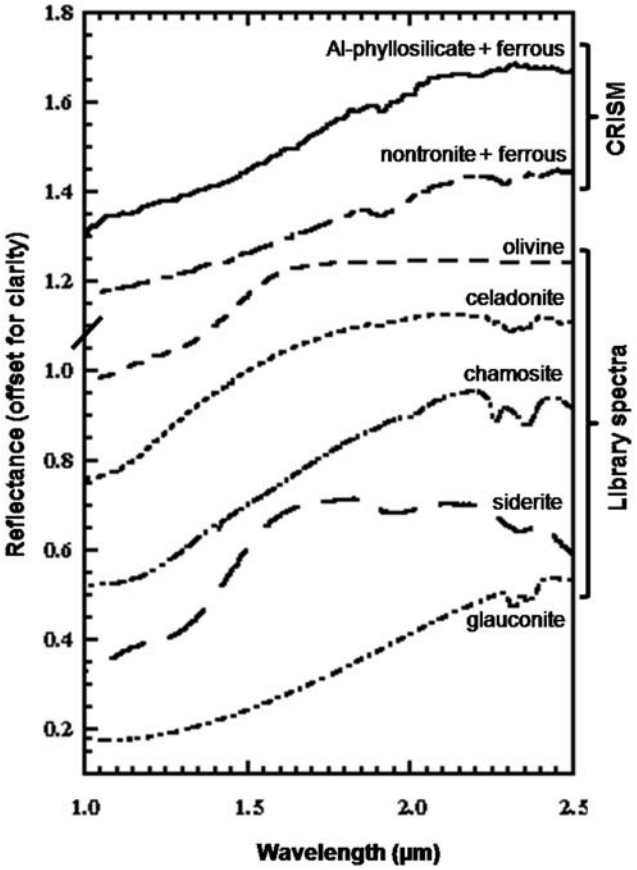

Figure 15. CRISM spectra with ferrous slope (Al-phyllosilicate + ferrous and nontronite + ferrous) compared to library spectra of ferrous phyllosilicates (celadonite, glauconite), a ferrous carbonate (chamosite, siderite), and a ferrous olivine (olivine).

absorption at 1.25 μm [*Gaffey et al.*, 1993; *Sunshine and Pieters*, 1998]. A ferrous mica such as celadonite or glauconite or a chlorite such as chamosite (see *Bishop et al.* [2008a] for spectral properties) is most likely to be causing this feature because they form under conditions similar to the clay minerals observed at Mawrth Vallis. However, the micas have weak absorptions near 2.2–2.35 μm that we have not observed in CRISM spectra.

4.3. Stratigraphy

[26] The nontronite-bearing unit is the lowermost layer, is indurated but non cliff forming, and is unconformably overlain by the Al-phyllosilicate unit (Figure 16) [e.g., *Wray et al.*, 2008]. The unit underlying the nontronite is not observed in most cases and therefore we cannot constrain the thickness of the nontronite unit. The upper ~10 m of the nontronite unit typically contains a ferrous component characterized by the addition of the increasing slope from 1 to 2 μm and is sometimes accompanied by a weakening of the characteristic nontronite bands. The Al-phyllosilicate unit is an indurated, easily friable unit ~40 m thick, as determined using HRSC Digital Elevation Models [*Wray et al.*, 2008], that forms cliffs and buttes but does not shed boulders and is finely layered at HiRISE resolutions (~0.3 m/pixel). Within this unit are two distinct layers: a lower layer composed mainly of montmorillonite and hydrated silica and an upper layer composed of kaolinite and hydrated silica (Figure 16). The montmorillonite-bearing portion with a ferrous slope located at the boundary with the underlying nontronite unit texturally resembles the rest of the Al-phyllosilicate unit. The kaolinite-bearing layer appears to be much thinner than the montmorillonite-bearing layer, usually spanning areas <50 m across. The uppermost layer is a spectrally unremarkable cliff-forming unit a few meters in thickness (Noe Dobrea et al., submitted manuscript, 2009), likely volcanic in origin, that sheds boulders and drapes the underlying terrain. This stratigraphy is generally consistent throughout the Mawrth Vallis region; however, there are some localities that deviate from this stratigraphy [*Wray et al.*, 2008; Noe Dobrea et al., submitted manuscript, 2009]. For more detail on the morphology of the phyllosilicate units, see Noe Dobrea et al. (submitted manuscript, 2009).

5. Implications for Depositional Environment and Past Climate

[27] Clay minerals form in aqueous environments through many mechanisms. At Mawrth Vallis, however, we are constrained by both the size of the deposit and its uniformity: several hundred meters of clay-bearing rocks in the same stratigraphy across 1×10^6 km^2 (Noe Dobrea et al., submitted manuscript, 2009). Therefore, we only consider formational mechanisms that can account for similar alteration across this large area. The unconformity between the nontronite-bearing unit and the Al-phyllosilicate unit indicates two periods of formation [*Wray et al.*, 2008]. Additionally deposition of the layered units and their alteration to hydrated silicates may result from distinct processes. The three scenarios discussed (ashfall, sedimentary deposition, and pedogenesis) can apply to both units.

5.1. Ashfall Deposit

[28] The most likely formational mechanism for the Al-clay-bearing unit is in situ alteration of a volcanic ash deposit, analogous to bentonite formation commonly observed on Earth. Bentonitic montmorillonites are one of the most common alteration products of volcanic ash [*Hewett*, 1917; *Keller*, 1970; *Ross and Shannon*, 1926; *Wherry*, 1917]. Nontronite also forms from alteration of volcanic glass, found in ash or pyroclastic deposits [*Hein and Scholl*, 1978]. An ash deposit would drape the underlying terrain, as has been observed for the Al-phyllosilicate-bearing unit [*Wray et al.*, 2008], and the layering observed in both the Al- and Fe/Mg-phyllosilicate units could be explained by several ashfall events. However, there is no volcanic source in the region. Volcanic ash can travel planet-wide if the eruption is large enough, so it is possible that an eruption farther away could be the source of the ash.

[29] Ashfall deposits can alter either through groundwater circulation or by direct deposition into an open body of water, as in the case of some bentonites [*Grim and Güven*, 1978]. Given the common, widespread occurrence of bentonites on Earth, it is likely that no special conditions are required in its formation, beyond significant water (either marine or nonmarine) with active Mg, Fe, and silica in order to form montmorillonite [*Keller*, 1956, 1970; *Ross and*

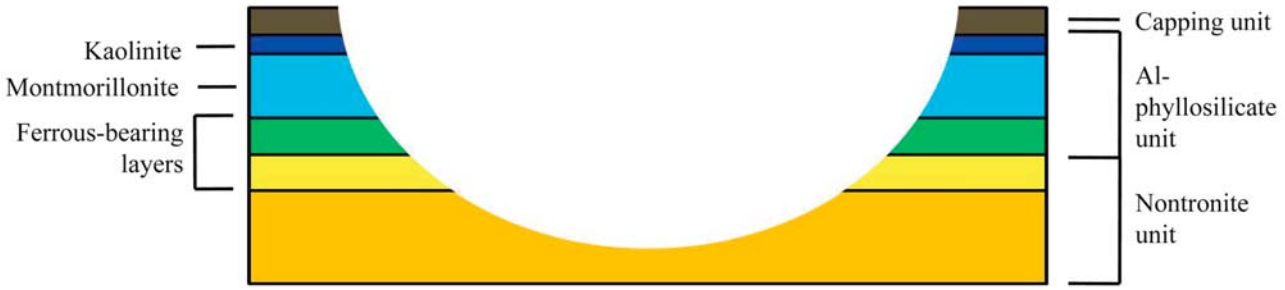

Figure 16. A sample stratigraphy of the Mawrth Vallis region. Orientation of the beds and their contacts are not representative. Orange, nontronite; yellow, nontronite with a ferrous component; green, montmorillonite/hydrated silica with a ferrous component; light blue, montmorillonite + hydrated silica; dark blue, kaolinite + hydrated silica; brown, spectrally unremarkable capping unit. The orange and yellow layers are the nontronite unit, and the green, light blue, and dark blue layers make up the Al-phyllosilicate unit. The yellow and green layers contain the ferrous component identified near the boundary between the nontronite and Al-phyllosilicate units. The capping unit drapes the Al-phyllosilicate unit, which unconformably overlies the nontronite-bearing unit [*Michalski and Noe Dobrea*, 2007; *Wray et al.*, 2008].

Shannon, 1926]. Thus, extensive groundwater or an open body of water is required.

5.2. Sedimentary Deposition

[30] In this scenario, the clay minerals formed elsewhere and were transported to the Mawrth Vallis region in a large fluvial-lacustrine or marine environment. This would result in layering within the units and can account for the volume of sediment. The separate layers within a unit may contain different abundances of phyllosilicates, but that is below the resolution of CRISM. An Earth analog might be the extensive clay-bearing deposits in the American southwest which were sourced in volcanic regions to the south [*Ash*, 1987]. Another analog could be the extensive clay deposits in oceanic basins, of which smectites are the dominant clay species [*Cole and Shaw*, 1983].

[31] Clay deposits in marine sedimentary basins typically reflect climate conditions of landmasses adjacent to the basin because there is little to no diagenetic alteration experienced after deposition, as long as the deposits are buried less than 2–3 km and have not been significantly modified by volcanic/hydrothermal processes [*Chamley*, 1989; *Cole and Shaw*, 1983]. On Earth, smectites are the dominant clay mineral in the Pacific, Indian, and South Atlantic oceanic sediments. Nontronite is the most common authigenic smectite in these settings, followed by montmorillonite and saponite [*Cole and Shaw*, 1983]. Given that nontronite (a smectite) is present as the lowermost layer, indicative of a hydrolytic, warm/wet environment, progression upward through an Al-rich smectite (montmorillonite) into kaolinite would indicate an increasingly warmer, wetter climate since kaolinite is an indicator of intense chemical weathering in a warm/wet climate [*Cole and Shaw*, 1983; *Keller*, 1970].

5.3. Pedogenesis

[32] Pedogenesis is soil formation and typically occurs from the top down as gravity drives water flowing through the rock, replenished by precipitation. This process removes heavier ions first, transporting Mg and Fe before Al and Si [*Keller*, 1970]. Clay minerals are a primary product of soil formation from a volcanic parent rock [*Righi and Meunier*, 1995]. The first clay alteration product is nontronite, an iron-bearing smectite. As more water transports the Fe away, montmorillonite (Al-bearing smectite) is formed at the top of the profile. As alteration continues, kaolinite, other kaolin family minerals, and gibbsite are formed at the top of the profile and montmorillonite continues to form deeper, replacing the nontronite [*Righi and Meunier*, 1995]. The stratigraphic profile observed at Mawrth Vallis is consistent with this type of soil profile: nontronite at the bottom, overlain by montmorillonite, with kaolinite at the top. The montmorillonite at Mawrth Vallis could have formed either through alteration of volcanic parent rocks or through leaching of previously altered Fe/Mg-smectite-bearing rocks. However, pedogenesis is more likely to have formed the Al-phyllosilicate-bearing unit than the nontronite-bearing unit. In order to alter the known thickness of the nontronite-bearing unit (~100 m) a large volume of water would be needed to flow down and through this thickness which would result in Al-phyllosilicates forming at the top of this unit (separate from the Al-phyllosilicate unit).

[33] Pedogenesis in a cool/wet climate will produce secondary silica phases such as opal, with kaolinite present at the top of the column and smectites present at the bottom, if they were present in the parent rock. This process, known as podzolization, typically occurs in the middle-to-high northern latitudes on Earth [*Chamley*, 1989]. However, it typically produces clay horizons on the order of tens of centimeters, not tens of meters like we are seeing in Mawrth; therefore, this is a less likely climate scenario.

[34] Pedogenesis in a temperate or tropical climate will produce laterites with much thicker clay horizons due to higher temperatures and much higher annual rainfall. Laterite formation is a more probable scenario than podzolization given the thickness of the clay-bearing units at Mawrth Vallis. However, extensive pedogenesis removes the structures of the parent rock such as layering [*Righi and Meunier*, 1995]. In Mawrth Vallis, the Al-phyllosilicate-bearing unit does contain layers, making this a less likely scenario for the alteration of the entire stratigraphic column. However, it is possible that the top portion of the Al-phyllosilicate unit was leached pedogenically, forming kaolinite in the top portions and transporting any Si and

residual Fe away, possibly depositing it lower in the stratigraphic section [*Keller*, 1970]. This would lead to the formation of hydrated silica and potentially a ferrous-bearing component.

5.4. Ferrous Component Formation

[35] The areally consistent, limited stratigraphic location of the ferrous slope in CRISM data supports an integrated component rather than a coating as the latter would occur wherever the rock was exposed to the altering chemistry. The presence of Fe^{2+} indicates either rapid deposition and/or a reducing environment. On Earth, aqueous Fe^{3+} is reduced by acidophilic bacteria [*Brock and Gustafson*, 1976; *Lowenstam*, 1981; *Nealson*, 1997]. However, bacteria are not required to reduce Fe^{3+}; certain compounds can also reduce Fe^{3+} when in aqueous solutions, such as ascorbic acid ($C_6H_8O_6$) and dithionite ($S_2O_4^{2-}$) [*Stucki et al.*, 1996]. Fe^{2+} is also deposited in marine hydrothermal systems below the ocean floor [*Schlegel and Jannasch*, 2006].

6. Summary

[36] This study expands our knowledge of the ancient terrain in the Mawrth Vallis region. We have confirmed and expanded observations by OMEGA, identifying nontronite, montmorillonite, hydrated silica, kaolinite, and a ferrous component through their distinct spectral characteristics. In some locations, the Fe-OH ~2.29 μm feature in nontronite is shifted to 2.30 μm, indicating there has been some Mg substitution. Nontronite/Fe-Mg-smectite has been consistently identified in the lowermost unit. This unit is unconformably overlain by a unit containing montmorillonite and hydrated silica, with a layer of kaolinite and hydrated silica at the top of this second unit. It is likely there are other minerals in these units such as plagioclase that have no spectral features in the 1.0–2.5 μm region; plagioclase has been identified in TIR data and suggested in spectral models. This same stratigraphy has been observed across 1×10^6 km^2, indicating a regional process formed these clay-bearing units. The most likely formation scenario is that layers of volcanic ash were altered by groundwater circulation or after being deposited into a marine or lacustrine basin. The different mineralogies of the units can be accounted for if the ash deposits had different original compositions. It can also be accounted for by a change in water chemistry in the case of deposition into an open body of water. Other possibilities for the formation of these clay-bearing units include erosion, transportation, and deposition of sediments or in situ pedogenesis of volcanic or previously altered nontronite-bearing parent rocks. It is likely the alteration took place in a warm/wet climate because of the volume of altered material; however, if the alteration occurred after direct deposition into a marine environment (rather than during erosion and transport), then surface temperature did not play a role.

[37] **Acknowledgments.** Partial support to N.K.M. was provided by the Naval Post-graduate School Center for Remote Sensing, by the University Affiliated Research Center at UCSC, and by NASA's Mars Fundamental Research program. Additional support was provided by NASA's Mars Data Analysis program and the MRO/CRISM mission. Formal reviews by David Bish and Damien Loizeau greatly improved this paper. We would like to thank the MRO/CRISM Team for the collection and initial processing of the images and Frank Seelos, Olivier Barnouin-Jha, and team for creating the browse products available online at http://crism-map.jhuapl.edu/.

References

Amador, E. S., J. L. Bishop, N. K. McKeown, M. Parente, and J. T. Clark (2009), Detection of kaolinite at Mawrth Vallis, Mars: Analysis of laboratory mixtures and development of remote sensing parameters, *Lunar Planet. Sci.*, *XL*, Abstract 2188.

Anderson, J. H., and K. A. Wickersheim (1964), Near infrared characterization of water and hydroxyl groups on silica surfaces, *Surf. Sci.*, *2*, 252–260, doi:10.1016/0039-6028(64)90064-0.

Ash, S. R. (1987), Petrified Forest National Park, Arizona, in *Rocky Mountain Section of the Geological Society America*, *Centen. Field Guide*, edited by S. S. Beus, pp. 405–410, Geol. Soc. of Am., Boulder, Colo.

Beyer, R. A., and the HiRISE Team (2008), HiRISE photoclinometry of proposed MSL landing sites, *Lunar Planet. Sci.*, *XXXIX*, Abstract 2485.

Bibring, J.-P., et al. (2005), Mars surface diversity as revealed by the OMEGA/Mars Express observations, *Science*, *307*, 1576–1581, doi:10.1126/science.1108806.

Bibring, J.-P., Y. Langevin, J. F. Mustard, F. Poulet, R. Arvidson, A. Gendrin, B. Gondet, N. Mangold, P. Pinet, and F. Forget (2006), Global mineralogical and aqueous Mars history derived from OMEGA/Mars Express data, *Science*, *312*, 400–404, doi:10.1126/science.1122659.

Bishop, J. L., C. M. Pieters, and J. O. Edwards (1994), Infrared spectroscopic analyses on the nature of water in montmorillonite, *Clays Clay Miner.*, *42*, 702–716, doi:10.1346/CCMN.1994.0420606.

Bishop, J. L., E. Murad, M. D. Lane, and R. L. Mancinelli (2004), Multiple techniques for mineral identification on Mars: A study of hydrothermal rocks as potential analogues for astrobiology sites on Mars, *Icarus*, *169*, 311–323, doi:10.1016/j.icarus.2003.12.025.

Bishop, J. L., P. Schiffman, M. D. Lane, and M. D. Dyar (2005), Solfataric alteration in Hawaii as a mechanism for formation of the sulfates observed on Mars by OMEGA and the MER instruments, *Lunar Planet. Sci.*, *XXXVI*, Abstract 1456.

Bishop, J. L., et al. (2007), Layering of Al- and Fe/Mg-phyllosilicates in Western Mawrth Vallis, Mars, and implications for aqueous processes during the noachian period, *Eos Trans. AGU*, *88*(52), Fall Meet. Suppl., Abstract P13D-1559.

Bishop, J. L., M. D. Lane, M. D. Dyar, and A. J. Brown (2008a), Reflectance and emission spectroscopy study of four groups of phyllosilicates: Smectites, kaolinite-serpentines, chlorites and micas, *Clay Miner.*, *43*(1), 35–54, doi:10.1180/claymin.2008.043.1.03.

Bishop, J. L., et al. (2008b), Phyllosilicate diversity and past aqueous activity revealed at Mawrth Vallis, Mars, *Science*, *321*, 830–833, doi:10.1126/science.1159699.

Brock, T. D., and J. Gustafson (1976), Ferric iron reduction by sulfur- and iron-oxidizing bacteria, *Appl. Environ. Microbiol.*, *32*(4), 567–571.

Burns, R. G. (1993), *Mineralogical Applications of Crystal Field Theory*, 2nd ed., 551 pp., Cambridge Univ. Press, Cambridge, U. K.

Carr, M. H. (1996), *Water on Mars*, Oxford Univ. Press, New York.

Chabrillat, S., A. F. H. Goetz, L. Krosley, and H. W. Olsen (2002), Use of hyperspectral images in the identification and mapping of expansive clay soils and the role of spatial resolution, *Remote Sens. Environ.*, *82*, 431–445, doi:10.1016/S0034-4257(02)00060-3.

Chamley, H. (1989), *Clay Sedimentology*, 623 pp., Springer, New York.

Clark, R. N., T. V. V. King, M. Klejwa, and G. A. Swayze (1990), High spectral resolution reflectance spectroscopy of minerals, *J. Geophys. Res.*, *95*, 12,653–12,680, doi:10.1029/JB095iB08p12653.

Clark, R. N., G. A. Swayze, T. V. V. King, A. Gallagher, and W. M. Calvin (1993), Digital spectral library: Version 1, 0.2 to 3.0-μm, *U.S. Geol. Surv. Open File Rep. 93–592*.

Clark, R. N., G. A. Swayze, K. E. Livo, R. F. Kokaly, S. J. Sutley, J. B. Dalton, R. R. McDougal, and C. A. Gent (2003), Imaging spectroscopy: Earth and planetary remote sensing with the USGS Tetracorder and expert systems, *J. Geophys. Res.*, *108*(E12), 5131, doi:10.1029/2002JE001847.

Clark, R. N., G. A. Swayze, R. Wise, E. Livo, T. Hoefen, R. Kokaly, and S. J. Sutley (2007), USGS digital spectral library splib06a, *U.S. Geol. Surv. Digital Data Ser. 231*.

Cole, T. G., and H. F. Shaw (1983), The nature and origin of authigenic smectites in some recent marine sediments, *Clay Miner.*, *18*, 239–252, doi:10.1180/claymin.1983.018.3.02.

Craddock, R. A., and A. D. Howard (2002), The case for rainfall on a warm, wet early Mars, *J. Geophys. Res.*, *107*(E11), 5111, doi:10.1029/2001JE001505.

Craddock, R. A., and T. A. Maxwell (1990), Resurfacing of the Martian highlands in the Amenthes and Tyrrhena region, *J. Geophys. Res.*, *95*, 14,265–14,278, doi:10.1029/JB095iB09p14265.

Edgett, K. S., and T. J. Parker (1997), Water on early Mars: Possible subaqueous sedimentary deposits covering ancient cratered terrain in western Arabia and Sinus Meridiani, *Geophys. Res. Lett.*, *24*, 2897–2900, doi:10.1029/97GL02840.

Gaffey, S. J., L. A. McFadden, D. Nash, and C. M. Pieters (1993), Ultraviolet, visible, and near-infrared reflectance spectroscopy: Laboratory spectra of geologic materials, in *Remote Geochemical Analysis: Elemental and Mineralogical Composition*, edited by C. M. Pieters and P. A. J. Englert, pp. 43–77, Cambridge Univ. Press, Cambridge, U. K.

Gates, W. P. (2005), Infrared spectroscopy and the chemistry of dioctahedral smectites, in *The Application of Vibrational Spectroscopy to Clay Minerals and Layered Double Hydroxides*, edited by J. T. Kloprogge, pp. 125–168, Clay Miner. Soc., Aurora, Colo.

Golombek, M. P., J. Grant, A. R. Vasavada, M. Watkins, E. Z. Noe Dobrea, J. Griffes, and T. Parker (2008), Downselection of landing sites for the Mars science laboratory, *Lunar Planet. Sci.*, *XXXIX*, Abstract 2181.

Grim, R. E., and N. Güven (1978), *Bentonites: Geology, Mineralogy, Properties and Uses*, Elsevier, Amsterdam.

Harrison, K. P., and R. E. Grimm (2005), Groundwater-controlled valley networks and the decline of surface runoff on early Mars, *J. Geophys. Res.*, *110*, E12S16, doi:10.1029/2005JE002455.

Hein, J. R., and D. W. Scholl (1978), Diagenesis and distribution of late Cenozoic volcanic sediment in the southern Bering Sea, *Geol. Soc. Am. Bull.*, *89*, 197–210, doi:10.1130/0016-7606(1978)89<197:DADOLC>2.0.CO;2.

Hewett, D. F. (1917), The origin of bentonite, *J. Wash. Acad. Sci.*, *7*, 196–198.

Hunt, G. R. (1977), Spectral signatures of particulate minerals in the visible and near infrared, *Geophysics*, *42*(3), 501–513, doi:10.1190/1.1440721.

Keller, W. D. (1956), Clay minerals as influenced by environments of their formation, *Am. Assoc. Pet. Geol. Bull.*, *40*(11), 2689–2710.

Keller, W. D. (1970), Environmental aspects of clay minerals, *J. Sediment. Petrol.*, *40*(3), 788–854.

Lear, P. R., P. Komadel, and J. W. Stucki (1988), Mossbauer spectroscopic identification of iron oxides in nontronite from Hohen Hagen, Federal Republic of Germany, *Clays Clay Miner.*, *36*, 376–378, doi:10.1346/CCMN.1988.0360414.

Loizeau, D., et al. (2007), Phyllosilicates in the Mawrth Vallis region of Mars, *J. Geophys. Res.*, *112*, E08S08, doi:10.1029/2006JE002877.

Loizeau, D., N. Mangold, F. Poulet, V. Ansan, E. Hauber, J.-P. Bibring, B. Gondet, Y. Langevin, P. Masson, and G. Neukum (2009), Stratigraphy in the Mawrth Vallis region through OMEGA, HRSC color imagery and DTM, *Icarus*, in press.

Lowenstam, H. A. (1981), Minerals formed by organisms, *Science*, *211*, 1126–1131, doi:10.1126/science.7008198.

Masursky, H. (1973), An overview of geologic results of Mariner 9, *J. Geophys. Res.*, *78*, 4009–4030, doi:10.1029/JB078i020p04009.

McKeown, N. K., et al. (2007), Phyllosilicate identification in Mawrth Vallis: An analysis of CRISM multispectral data and targeted images FRT4ECA and HRS307A, *Eos Trans. AGU*, *88*(52), Fall Meet. Suppl., Abstract P13D-1558.

McKeown, N. K., J. L. Bishop, J. Cuadros, E. Amador, and E. A. Silver (2008), Characterization of phyllosilicate units at Mawrth Vallis: Comparison of CRISM observations and intimate phyllosilicate mixtures, paper presented at Workshop on Martian Phyllosilicates: Recorders of Aqueous Processes, Cent. Natl. d'Etud. Spatiales, Paris.

Michalski, J. R., and R. L. Fergason (2009), Composition and thermal inertia of the Mawrth Vallis region of Mars from TES and THEMIS data, *Icarus*, *199*, 25–48, doi:10.1016/j.icarus.2008.08.016.

Michalski, J. R., and E. Z. Noe Dobrea (2007), Evidence for a sedimentary origin of clay minerals in the Mawrth Vallis region, Mars, *Geology*, *35*(10), 951–954, doi:10.1130/G23854A.1.

Milliken, R. E., et al. (2008), Opaline silica in young deposits on Mars, *Geology*, *36*(11), 847–850, doi:10.1130/G24967A.1.

Moll, W. F. J. (2001), Baseline studies of the clay minerals society source clays: Geologic origin, *Clays Clay Miner.*, *49*, 374–380, doi:10.1346/CCMN.2001.0490503.

Morris, R. V., et al. (2000), Mineralogy, composition, and alteration of Mars Pathfinder rocks and soils: Evidence from multispectral, elemental, and magnetic data on terrestrial analogue, SNC meteorite, and Pathfinder samples, *J. Geophys. Res.*, *105*, 1757–1817, doi:10.1029/1999JE001059.

Murchie, S., et al. (2007), Compact Reconnaissance Imaging Spectrometer for Mars (CRISM) on Mars Reconnaissance Orbiter (MRO), *J. Geophys. Res.*, *112*, E05S03, doi:10.1029/2006JE002682.

Murchie, S. L., et al. (2009), Compact Reconnaissance Imaging Spectrometer investigation and data set from the Mars Reconnaissance Orbiter's primary science phase, *J. Geophys. Res.*, *114*, E00D07, doi:10.1029/2009JE003344.

Mustard, J. F., et al. (2008), Hydrated silicate minerals on Mars observed by the Mars Reconnaissance Orbiter CRISM instrument, *Nature*, *454*, 305–309, doi:10.1038/nature07097.

Nealson, K. (1997), The limits of life on Earth and searching for life on Mars, *J. Geophys. Res.*, *102*, 23,675–23,686, doi:10.1029/97JE01996.

Noe Dobrea, E. Z., et al. (2007), The extent of phyllosilicates in the northern highlands around Mawrth Vallis: CRISM observations of western Arabia Terra, *Eos Trans. AGU*, *88*(52), Fall Meet. Suppl., Abstract P13D-1560.

Noe Dobrea, E. Z., et al. (2008), Clay bearing units in the region around Mawrth Vallis: Stratigraphy, extent, and possible alteration fronts, *Lunar Planet. Sci.*, *XXXIX*, Abstract 1077.

Parente, M. (2008), A new approach to denoising CRISM images, *Lunar Planet. Sci.*, *XXXIX*, Abstract 2528.

Parente, M., J. L. Bishop, and J. Cuadros (2008), Lab experiments to simulate coatings on phyllosilicate rocks and comparison with CRISM data of Mars, paper presented at Martian Phyllosilicates: Recorders of Aqueous Processes, Cent. Natl. d'Etud. Spatiales, Paris, Abstract 7039.

Pelkey, S. M., et al. (2007), CRISM multispectral summary products: Parameterizing mineral diversity on mars from reflectance, *J. Geophys. Res.*, *112*, E08S14, doi:10.1029/2006JE002831.

Petit, S., J. Madejova, A. Decarreau, and F. Martin (1999), Characterization of octahedral substitutions in kaolinites using near infrared spectroscopy, *Clays Clay Miner.*, *47*, 103–108, doi:10.1346/CCMN.1999.0470111.

Pieri, D. (1976), Distribution of small channels on the Martian surface, *Icarus*, *27*, 25–50, doi:10.1016/0019-1035(76)90182-2.

Pieri, D. C. (1980), Martian valleys: Morphology, distribution, age, and origin, *Science*, *210*, 895–897, doi:10.1126/science.210.4472.895.

Pollack, J. B. (1979), Climatic change on the terrestrial planets, *Icarus*, *37*, 479–553, doi:10.1016/0019-1035(79)90012-5.

Pollack, J. B., J. F. Kasting, S. M. Richardson, and K. Poliackoff (1987), The case for a warm, wet climate on early Mars, *Icarus*, *71*, 203–224, doi:10.1016/0019-1035(87)90147-3.

Poulet, F., J. Bibring, J. F. Mustard, A. Gendrin, N. Mangold, Y. Langevin, R. E. Arvidson, B. Gondet, and C. Gomez (2005), Phyllosilicates on Mars and implications for the early Mars history, *Nature*, *438*, 623–627, doi:10.1038/nature04274.

Poulet, F., N. Mangold, D. Loizeau, J.-P. Bibring, Y. Langevin, J. R. Michalski, and B. Gondet (2008), Abundance of minerals in the phyllosilicate-rich units on Mars, *Astron. Astrophys.*, *487*, L41–L44, doi:10.1051/0004-6361:200810150.

Righi, D., and A. Meunier (1995), Origin of clays by rock weathering and soil formation, in *Origin and Mineralogy of Clays*, edited by B. Velde, pp. 43–161, Springer, Berlin.

Ross, C. S., and E. V. Shannon (1926), The minerals of bentonite and related clays and their physical properties, *J. Am. Ceram. Soc.*, *9*(2), 77–96, doi:10.1111/j.1151-2916.1926.tb18305.x.

Ruff, S. W., and V. E. Hamilton (2009), New insights into the nature of mineralogic alteration on Mars from orbiter, rover, and laboratory data, *Lunar Planet. Sci.*, *XL*, Abstract 2160.

Schlegel, H. G., and H. W. Jannasch (2006), Prokaryotes and their habitats, in *The Prokaryotes*, edited by M. Dworkin et al., pp. 137–184, Springer, New York.

Scott, D. H., and K. L. Tanaka (1986), Geologic map of western equatorial region of Mars, *U.S. Geol. Surv. Misc. Invest. Map*, *I-1802-A*.

Sherman, D. M., and N. Vergo (1988), Optical (diffuse reflectance) and Mössbauer spectroscopic study of the nontronite and related Fe-bearing smectites, *Am. Mineral.*, *73*, 1346–1354.

Squyres, S. W., and J. F. Kasting (1994), Early Mars: How warm and how wet?, *Science*, *265*, 744–749, doi:10.1126/science.265.5173.744.

Stucki, J. W., G. W. Bailey, and H. Gan (1996), Oxidation-reduction mechanisms in iron-bearing phyllosilicates, *Appl. Clay Sci.*, *10*, 417–430, doi:10.1016/0169-1317(96)00002-6.

Sunshine, J. M., and C. M. Pieters (1998), Determining the composition of olivine from reflectance spectroscopy, *J. Geophys. Res.*, *103*, 13,675–13,688, doi:10.1029/98JE01217.

Wherry, E. T. (1917), Clay derived from volcanic dust in the Pierre of South Dakota, *J. Wash. Acad. Sci.*, *7*, 576–583.

Wray, J. J., B. L. Ehlmann, S. W. Squyres, J. F. Mustard, and R. L. Kirk (2008), Compositional stratigraphy of layered deposits at Mawrth Vallis, Mars, *Geophys. Res. Lett.*, *35*, L12202, doi:10.1029/2008GL034385.

J.-P. Bibring, Institut d'Astrophysique Spatiale, Université Paris Sud, CNRS, F-91405 Orsay, France.

J. L. Bishop, NASA Ames Research Center, Moffett Field, CA 94035, USA.

B. L. Ehlmann and J. F. Mustard, Department of Geological Sciences, Brown University, Providence, RI 02912, USA.

N. K. McKeown and E. A. Silver, Department of Earth and Planetary Sciences, University of California, Santa Cruz, CA 95064, USA.

S. L. Murchie, Johns Hopkins University Applied Physics Laboratory, Laurel, MD 20723, USA.

E. Z. Noe Dobrea, Jet Propulsion Laboratory, California Institute of Technology, Pasadena, CA 91109, USA.

M. Parente, Department of Electrical Engineering, Stanford University, Stanford, CA 94305, USA.

G. A. Swayze, U.S. Geological Survey, Denver, CO 80225, USA.